

Learning Discretized Neural Networks under Ricci Flow

Jun Chen

JUNC@ZJU.EDU.CN

*Institute of Cyber-Systems and Control
Zhejiang University
Hangzhou, 310027, China*

Hanwen Chen

CHENHANWEN@ZJU.EDU.CN

*Institute of Cyber-Systems and Control
Zhejiang University
Hangzhou, 310027, China*

Mengmeng Wang

MENGMENGWANG@ZJU.EDU.CN

*Institute of Cyber-Systems and Control
Zhejiang University
Hangzhou, 310027, China*

Guang Dai

GUANG.GDAI@GMAIL.COM

State Grid Corporation of China

Yong Liu

YONGLIU@IPC.ZJU.EDU.CN

*Institute of Cyber-Systems and Control
Zhejiang University
Hangzhou, 310027, China*

Abstract

In this paper, we consider Discretized Neural Networks (DNNs) consisting of low-precision weights and activations, which suffer from either infinite or zero gradients caused by the non-differentiable discrete function in the training process. In this case, most training-based DNNs use the standard Straight-Through Estimator (STE) to approximate the gradient w.r.t. discrete values. However, the STE will cause the problem of gradient mismatch, which implies that the approximated gradient is with perturbations. We propose an analysis that this mismatch can be viewed as a metric perturbation in a Riemannian manifold through the lens of duality theory. To address this problem, based on the information geometry, we construct the Linearly Nearly Euclidean (LNE) manifold for DNNs as a background to deal with perturbations. By introducing a partial differential equation on metrics, the Ricci flow, we prove the dynamical stability and convergence of the LNE metric with the L^2 -norm perturbation. And unlike the previous perturbation theory which gives the rate of convergence is the fractional powers, we yield the metric perturbation under the Ricci flow can be exponentially decayed in the LNE manifold. The experimental results on various datasets demonstrate that our method achieves better and more stable performance for DNNs than other representative training-based methods.

Keywords: Discretized Neural Networks, Gradient Perturbation, Information Geometry, Ricci Flow, Riemannian Manifold

1. Introduction

Discretized neural networks (Courbariaux et al., 2016; Li et al., 2016; Zhu et al., 2016) have been proven to be efficient in computing, which can significantly reduce computa-

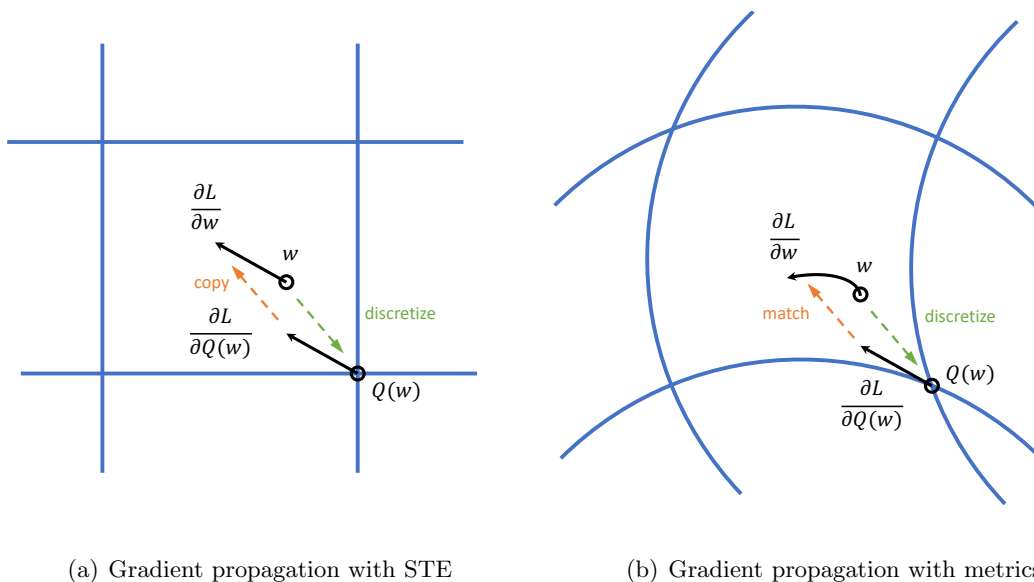


Figure 1: Comparison of STE and our method. We denote the arrows and points as gradients and weights, respectively. In particular, when a point falls on the grid point, it means that the weight is discretized at this time. In the forward of DNNs, the continuous weight \mathbf{w} is mapped to a discrete weight $Q(\mathbf{w})$ via a discrete function. In the backward, the gradient is propagated from $\partial L/\partial Q(\mathbf{w})$ to $\partial L/\partial \mathbf{w}$. (a) The STE simply copies the gradient, i.e., $\partial L/\partial \mathbf{w} = \partial L/\partial Q(\mathbf{w})$. (b) Our method, on the other hand, matches the gradient by introducing the proper metric $g_{\mathbf{w}}$, i.e., $\partial L/\partial \mathbf{w} = g_{\mathbf{w}}^{-1} \partial L/\partial Q(\mathbf{w})$, while taking into account the gradient mismatch caused by STE in a Riemannian manifold.

tional complexity, storage space, power consumption, resources, etc (Chen et al., 2020). Considering a DNN which is able to be well-trained, based on the standard chain rule, the gradient w.r.t. the continuous weight¹ \mathbf{w} propagating through a discrete function $Q(\cdot)$, i.e., $\frac{\partial L}{\partial \mathbf{w}} = \frac{\partial L}{\partial Q(\mathbf{w})} \frac{\partial Q(\mathbf{w})}{\partial \mathbf{w}}$, suffers from either infinite or zero derivatives. Its root is that the derivative $\partial Q(\mathbf{w})/\partial \mathbf{w}$ can not be calculated. In the backward, one can obtain the gradient $\partial L/\partial Q(\mathbf{w})$, but need to update the continuous weight \mathbf{w} via the gradient $\partial L/\partial \mathbf{w}$. Since the gradient $\partial L/\partial \mathbf{w}$ can not be obtained explicitly, one needs the derivative $\partial Q(\mathbf{w})/\partial \mathbf{w}$ as a bridge to calculate $\partial L/\partial \mathbf{w}$ via the chain rule.

In order to address the problem of either infinite or zero gradients caused by the non-differentiable discrete function, Hinton (2012) first proposed the Straight-Through Estimator (STE) that yields an immediate connection between $\partial L/\partial \mathbf{w}$ and $\partial L/\partial Q(\mathbf{w})$ in back-propagation such that bypassing the derivative $\partial Q(\mathbf{w})/\partial \mathbf{w}$. The definition of STE was then given by Bengio et al. (2013), which can be summarized as: the gradient w.r.t. the discretized weight can be approximated by the gradient w.r.t. the continuous weight with

1. In this paper, the continuous weight is relative to the neural network (its data type is full-precision). And the discretized weight is relative to the discretized neural network (its data type is low-precision).

clipping, as shown in Figure 1 (a). Subsequently, Courbariaux et al. (2016) applied STE to binarized neural networks as it provides an approximated gradient:

$$\frac{\partial L}{\partial \mathbf{w}} = \frac{\partial L}{\partial \text{sign}(\mathbf{w})} \cdot \mathbb{I}, \quad \text{where } \mathbb{I} := \begin{cases} 1 & \text{if } |\mathbf{w}| \leq 1 \\ 0 & \text{otherwise} \end{cases}, \quad (1)$$

where \mathbb{I} is the indicator function (Courbariaux et al., 2016). Note that $Q(\cdot)$ will degenerate to $\text{sign}(\cdot)$ which is equal to $+1$ for $\mathbf{w} \geq 0$ and -1 otherwise in binarized neural networks. As STE had been successfully implemented in the training of binarized neural networks, it continued to be extended to ternary neural networks (Li et al., 2016) and arbitrary bit-width discretized neural networks (Zhou et al., 2016).

On the other hand, Non-STE methods consist in all techniques that do not rely on STE, e.g., (Hou et al., 2016; Bai et al., 2018; Leng et al., 2018). However, the learning process of Non-STE methods depends heavily on hyper-parameters (Chen et al., 2019), such as weight partition portion in each iteration (Zhou et al., 2017) and penalty setting in tuning (Leng et al., 2018). Hence, STE methods are widely used in DNNs rather than Non-STE methods because of their simplicity and versatility.

As STE is introduced into DNNs, however, it inevitably brings the problem of *gradient mismatch*: the gradient w.r.t. the continuous weight is not strictly equal to the gradient w.r.t. the discretized weight when $|\mathbf{w}| \leq 1$ (Chen et al., 2019), which compromises the training stability of DNNs (Cai et al., 2017; Liu et al., 2018; Qin et al., 2020). Starting from the formula of STE, it seems that this problem is able to be alleviated by modifying the gradient $\partial L / \partial \mathbf{w}$.

Zhou et al. (2016) proposed to first transform the weight \mathbf{w} into the new one $\tilde{\mathbf{w}}$ via

$$\tilde{\mathbf{w}} = \frac{\tanh(\mathbf{w})}{\max(|\tanh(\mathbf{w})|)}.$$

By discretizing the new weight $\tilde{\mathbf{w}}$, the STE then acts on $\tilde{\mathbf{w}}$. During back-propagation, the gradient can be further computed as follows

$$\frac{\partial L}{\partial \mathbf{w}} = \frac{\partial L}{\partial Q(\tilde{\mathbf{w}})} \frac{1 - \tanh^2(\mathbf{w})}{\max(|\tanh(\mathbf{w})|)}.$$

The purpose of the authors is to manually redefine the indicator function \mathbb{I} as $\frac{1 - \tanh^2(\mathbf{w})}{\max(|\tanh(\mathbf{w})|)}$ such that the function $\frac{1 - \tanh^2(\mathbf{w})}{\max(|\tanh(\mathbf{w})|)}$ provides a smooth transition to avoid abrupt clipping of the indicator function near ± 1 . It is remarkable that Chen et al. (2019) proposed to learn $\partial L / \partial \mathbf{w}$ by a neural network, e.g., fully-connected layers or LSTM (Sak et al., 2014). Their specific approach is to use neural networks as a shared meta quantizer M_ϕ parameterized by ϕ across layers to replace the gradient via:

$$\frac{\partial L}{\partial \mathbf{w}} = M_\phi \left(\frac{\partial L}{\partial Q(\mathbf{w})}, \bar{\mathbf{w}} \right) \frac{\partial \bar{\mathbf{w}}}{\partial \mathbf{w}},$$

where $\bar{\mathbf{w}}$ is the weight from the meta quantizer. With the input of the gradient $\partial L / \partial Q(\mathbf{w})$, the meta quantizer will output a new gradient to match $\partial L / \partial \mathbf{w}$ by updating the weight $\bar{\mathbf{w}}$ in the training process.

Recently, Ajanthan et al. (2021) formulated the binarization of neural networks as a constrained optimization problem by introducing a mirror descent framework (Beck and Teboulle, 2003) to perform gradient descent in the dual space (unconstrained space) with gradients computed in the primal space (discrete space). In particular, by projecting \mathbf{w} in the primal space into $\tilde{\mathbf{w}} = \tanh(\beta_k \mathbf{w})$ in the dual space, the gradient yields

$$\frac{\partial L}{\partial \mathbf{w}} = \frac{\partial L}{\partial \tilde{\mathbf{w}}} (1 - \tanh^2(\beta_k \mathbf{w})).$$

As the hyper-parameter $\beta_k \rightarrow \infty$, $\tilde{\mathbf{w}}$ gradually approaches $\text{sign}(\mathbf{w})$ until the corresponding neural network is fully binarized with an adaptive mirror map.

However, Zhou et al. (2016) obtained the new weight by manually setting the function \tanh , which can only scale the gradient as a whole and do not fundamentally alleviate the gradient mismatch. On the other hand, although Chen et al. (2019) automatically matched the gradient by learning a new neural network (a meta quantizer), the additional errors are also introduced to the gradient propagation to intensify the problem of gradient mismatch because of the introduction of the meta quantizer. Subsequently, Ajanthan et al. (2021) bypassed the problem of gradient mismatch because the derivative $\partial \tilde{\mathbf{w}} / \partial \mathbf{w} = (1 - \tanh^2(\beta_k \mathbf{w}))$ can be calculated directly, which implies that this method does not maintain discrete weights during the training. By now, the problem of gradient mismatch remains to be solved.

1.1 Contributions

In this work, we regard the gradient mismatch between $\partial L / \partial \mathbf{w}$ and $\partial L / \partial Q(\mathbf{w})$ as a perturbation phenomenon between these two gradients. By introducing the framework of Riemannian geometry in Figure 1 (b), the gradient mismatch is further viewed as a metric perturbation in a Riemannian manifold (Section 2.2) through the lens of duality theory (Amari and Nagaoka, 2000; Amari, 2016). As a partial differential equation on metrics, the Ricci flow (Sheridan and Rubinstein, 2006), is introduced, the metric perturbation can be exponentially decayed in theory such that the problem of gradient mismatch is theoretically solved. The main contributions of this paper are summarized in the following four aspects:

- We propose the LNE manifold endowed with the LNE metric (a special form of Ricci-flat metrics). According to the information geometry (Amari, 2016), we construct LNE manifolds for neural networks as a background to deal with perturbations.
- We prove the stability of LNE manifolds under the Ricci-DeTurck flow with the L^2 -norm perturbation. In this way, any Ricci flow starting close to the LNE metric exists for all time and converges to the LNE metric. And unlike the previous perturbation theory which gives the rate of convergence is the fractional powers ($t^{-3/2}$), we yield the metric perturbation under the Ricci flow can be exponentially decayed in the LNE manifold (e^{-t}).
- Based on the background of LNE manifolds, we propose the Ricci Flow Discretized Neural Network (RF-DNN) by defining a method for calculating the Ricci curvature

in such a way that the selection of coordinate systems is related to the input transformations of neural networks. In practice, the discrete Ricci flow is then introduced against the problem of gradient mismatch in DNNs.

- We carry out experiments on several classification benchmark datasets and network structures. Experimental results demonstrate the effectiveness of our geometric method RF-DNN compared with other representative training-based methods.

1.2 The Following Organization

This paper is organized as follows. In Section 2, we introduce the motivation and Ricci flow. According to the geometric structure measured by the LNE divergence, we deduce the corresponding LNE manifold for neural networks in Section 3. The stability of LNE manifolds under the Ricci-DeTurck is proved in Section 4. In Section 5, we calculate the approximated gradient in the LNE manifold to avoid solving the inverse of the LNE metric. In Section 6, we present how to introduce discrete Ricci flow into DNNs and yield the corresponding algorithm. The experimental results and ablation studies for RF-DNNs are presented in Section 7. Section 8 concludes the entire paper. Proofs are provided in the Appendices.

The Ricci flow on Ricci-flat metrics is known in the literature to be stable for C^0 perturbations in the L^∞ -norm (Section 2.4). Based on a Bregman divergence (Bregman, 1967), the LNE metric, a special form of Ricci-flat metrics, is introduced in neural networks via the LNE divergence (Theorem 9). Stability of LNE manifolds under the Ricci-DeTurck flow is then proved (Corollary 13 and Theorem 14). A discretization of the Ricci flow is therefore proposed, that leads to a practical algorithm (RF-DNNs, Algorithm 2).

2. Motivation and Formulation

2.1 Background

We start with the basic background for feed-forward DNNs that will be used throughout the paper. This background is on the basis of the work (Martens and Grosse, 2015).

A neural network can be regarded as a function to transform the input \mathbf{a}_0 into the output \mathbf{a}_l through a series of l layers. For the i -th layer ($i \in \{1, 2, \dots, l\}$), we denote \mathbf{W}_i as the weight matrix, \mathbf{s}_i as the vector of these weighted sum and \mathbf{a}_i as the vector of output (also known as the activation). Each layer receives vectors of a weighted sum of the input from the previous layer and computes their output via a nonlinear function.

For a DNN, we need to add a discrete function $Q(\cdot)$ to discretize the weight matrix \mathbf{W}_i and the activation vector \mathbf{a}_i . Furthermore, we mark the discretized weight matrix as $\hat{\mathbf{W}}_i = Q(\mathbf{W}_i)$ and the discretized activation vector as $\hat{\mathbf{a}}_i = Q(\mathbf{a}_i)$. Then the feed-forward of DNNs at each layer is given as follows:

$$\begin{aligned}
 \mathbf{s}_i &= \hat{\mathbf{W}}_i \hat{\mathbf{a}}_{i-1} \\
 \mathbf{a}_i &= f \odot \mathbf{s}_i \\
 \hat{\mathbf{a}}_i &= Q(\mathbf{a}_i)
 \end{aligned} \tag{2}$$

where f is a nonlinear (activation) function, \odot represents the element-wise multiplication. We vectorize $\hat{\mathbf{W}}_i$ as $\text{vec}(\hat{\mathbf{W}}_i)$ and stack their columns together, where $\text{vec}(\ast)$ is the operator that vectorizes a matrix as a column vector. Note that the vectorized weights in each layer before and after discretization are expressed as \mathbf{w} and $\hat{\mathbf{w}}$, respectively. We define the new discretized parameter vector as $\hat{\boldsymbol{\xi}} = \left[\text{vec}(\hat{\mathbf{W}}_1)^\top, \text{vec}(\hat{\mathbf{W}}_2)^\top, \dots, \text{vec}(\hat{\mathbf{W}}_l)^\top \right]^\top$, where we ignore the bias vector for brevity. Similarly, we can denote the parameter vector as $\boldsymbol{\xi} = \left[\text{vec}(\mathbf{W}_1)^\top, \text{vec}(\mathbf{W}_2)^\top, \dots, \text{vec}(\mathbf{W}_l)^\top \right]^\top$ where $\hat{\boldsymbol{\xi}} = Q(\boldsymbol{\xi})$.

In frequentist statistics, we represent the loss function as the negative log likelihood w.r.t. discretized parameter $\hat{\boldsymbol{\xi}}$, where the input $\mathbf{x} = \mathbf{a}_0$ can be observed. The way we minimize the loss function is to maximize the likelihood:

$$L(\mathbf{y}, \mathbf{z}) = -\log p(\mathbf{y}|\mathbf{z}, \hat{\boldsymbol{\xi}}) \quad (3)$$

where \mathbf{y} is the target and \mathbf{z} is the prediction computed by DNNs. Note that $p(\mathbf{y}|\mathbf{z}, \hat{\boldsymbol{\xi}})$ is the probability density function defined by the conditional probability distribution $P_{\mathbf{y}|\mathbf{z}}(\hat{\boldsymbol{\xi}})$ of DNNs. As for the back-propagation of DNNs, we explain it in later sections.

2.2 Motivation

We consider that the root of the gradient mismatch is that there is a perturbation phenomenon between $\partial L/\partial \mathbf{w}$ and $\partial L/\partial Q(\mathbf{w})$, i.e.,

$$\frac{\partial L}{\partial \mathbf{w}} = \mathcal{P} \left(\frac{\partial L}{\partial Q(\mathbf{w})} \right) \Big|_{O\left(\frac{\partial L}{\partial Q(\mathbf{w})}\right)} \quad (4)$$

where the input of the perturbation function \mathcal{P} is the gradient $\partial L/\partial Q(\mathbf{w})$, and the corresponding perturbation range is $O(\partial L/\partial Q(\mathbf{w}))$. If the perturbation range $O(\partial L/\partial Q(\mathbf{w}))$ can be eliminated or decayed, then there is an elegant solution to the problem of gradient mismatch. In the framework of perturbation theory of the linear space (Kato, 2013), it gives that the rate of convergence for perturbations is the fractional powers, e.g., $t^{-3/2}$.

Inspired by the mirror descent² framework (Beck and Teboulle, 2003), one can map the parameter from the primal space to the dual space, and compute the gradient in the dual space. When the Riemannian metric structures are introduced by means of information geometry (Amari, 2016), naturally³, the gradient mismatch is conclusively viewed as a metric perturbation in a Riemannian manifold. Specifically, with the help of Definition 1, the gradient $\partial L/\partial \mathbf{w}$ will be rewritten as $\tilde{\partial} L/\tilde{\partial} \mathbf{w}$ in a Riemannian manifold. Therefore,

2. Mirror descent induces non-Euclidean structure by solving iterative optimization problems using different proximity functions (Bubeck et al., 2015).

3. Natural gradient descent selects the steepest descent along a Riemannian manifold by multiplying the standard gradient by the inverse of the metric tensor (Amari, 1998). It is worth mentioning that mirror descent and natural gradient descent are proven to be equivalent to each other (Raskutti and Mukherjee, 2015), which implies that mirror descent is the steepest descent direction along the Riemannian manifold corresponding to the choice of Bregman divergence.

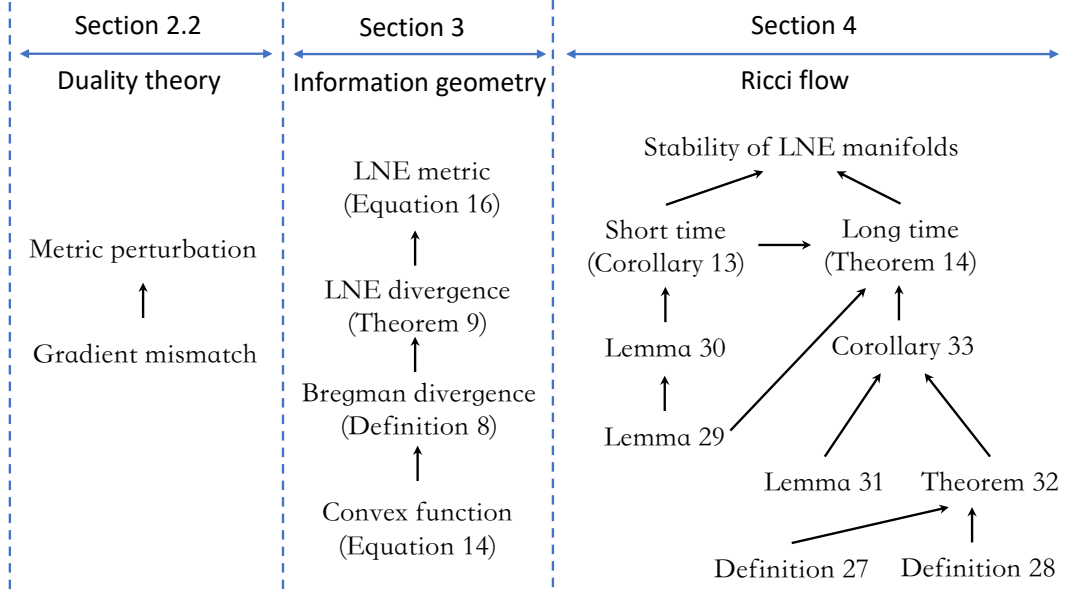


Figure 2: The overview of the theoretical ideas of this paper.

based on Equation (4), the problem of gradient mismatch can be defined as

$$\frac{\tilde{\partial}L}{\tilde{\partial}\mathbf{w}} = g_{\mathbf{w}}^{-1} \frac{\partial L}{\partial Q(\mathbf{w})} \quad (5)$$

where the perturbation item is implied in the metric $g_{\mathbf{w}}$. Then the metric perturbation phenomenon emerges, and the perturbation at this time is referred to the deviation from the original metric. In this way, we present the generalization of STE in a Riemannian manifold which will degenerate into the standard STE when the Riemannian metric g returns to the Euclidean metric δ .

Definition 1 (Amari, 1998) *The steepest descent direction of $L(\mathbf{w})$ in a Riemannian manifold, i.e., the **natural gradient descent**, is given by*

$$\tilde{\partial}L(\mathbf{w}) = g_{\mathbf{w}}^{-1} \partial L(\mathbf{w})$$

where $g^{-1} = (g^{ij})$ is the inverse of the metric $g = (g_{ij})$ and $\partial L(\mathbf{w})$ is the conventional gradient,

$$\partial L(\mathbf{w}) = \left[\frac{\partial L(\mathbf{w})}{\partial w_1}, \dots, \frac{\partial L(\mathbf{w})}{\partial w_n} \right]^\top.$$

Subsequently, a key question is what kind of manifolds we need to construct to deal with metric perturbations naturally and easily. Or what manifold is a “good” manifold in the presence of perturbations. In practice, it seems that general relativity gives an excellent example in nature to deal with small gravitational perturbations under the framework of a

Riemannian manifold (Wald, 2010). To treat the approximation in which gravity is “weak”, this means that the spacetime metric is nearly flat in the context of general relativity, which is enough for most cases, except for phenomena dealing with gravitational collapse and the large scale structure of the universe. By assuming the derivation γ_{ij} of the actual spacetime metric $g_{ij} = \eta_{ij} + \gamma_{ij}$ from a flat metric η_{ij} is “small”, the linearized gravity is presented to approximately compute the gravity in general relativity. An adequate definition of “smallness” in this context is that the components of γ_{ij} are much smaller than 1 in the global inertial coordinate system of η_{ij} . Such a linearly nearly flat metric greatly simplifies the calculation of “weak” gravity, and the manifolds constructed with such metrics are considered to be sufficient for approximating the manifold with perturbations.

Similarly, in this paper, by regarding the Euclidean metric δ_{ij} as the flat metric η_{ij} , we can naturally define the Linearly Nearly Euclidean (LNE) metric. If we can construct such a metric for DNNs, then a metric perturbation can be handled in the background of LNE manifolds. Motivated by the natural gradient descent (Amari, 2016) that connects neural networks with the Riemannian metric, LNE metrics can be mathematically constructed in neural networks. Specifically, our aim is to first introduce a convex function to derive the LNE divergence with the help of Bregman divergence (Bregman, 1967), and then construct the LNE metric by introducing the LNE divergence into a neural network⁴. Consequently, the LNE metric then appears in the gradient of the LNE manifold, similar to Definition 1. So far, all preparations have been completed, including the selection and construction of the manifold, and the only remaining problem is how to decay the metric perturbation based on a geometric tool: Ricci flow.

In Section 2.4, a series of proofs about the stability illustrates that the Ricci flow can decay the metric perturbation in the cases of Ricci-flat metrics. Therefore, as long as we can prove that a small perturbation of the LNE metric under the Ricci flow is decayed, the metric perturbation can be alleviated such that a theoretical solution for the problem of gradient mismatch in the training of DNNs is further given. And unlike the previous perturbation theory which gives the rate of convergence is the fractional powers, we yield the metric perturbation under the Ricci flow can be exponentially decayed in the LNE manifold, i.e., e^{-t} . In Figure 2, we give the overview of the theoretical ideas to facilitate sorting out the solution steps.

2.3 Ricci Flow

Definition 2 (Sheridan and Rubinstein, 2006) A **Riemannian metric** on a smooth manifold \mathcal{M} is a smoothly-varying inner product on the tangent space $T_p\mathcal{M}$ at each point $p \in \mathcal{M}$, i.e., a $(0,2)$ -tensor which is symmetric and positive-definite at each point of \mathcal{M} . One will usually write g for a Riemannian metric, and g_{ij} for its coordinate representation. A manifold together with a Riemannian metric, (\mathcal{M}, g) , is called a **Riemannian manifold**.

The concept of Ricci flow first published by Hamilton (Hamilton et al., 1982) on the Riemannian manifold \mathcal{M} of a time-dependent metric $g(t)$. Given the initial metric g_0 , the

4. The part from a convex function to the LNE divergence is in the mirror descent framework. Then, the part from the LNE divergence to the LNE metric introduces the idea of information geometry.

Ricci flow is a partial differential equation that evolves the metric tensor:

$$\begin{aligned}\frac{\partial}{\partial t}g(t) &= -2 \operatorname{Ric}(g(t)) \\ g(0) &= g_0\end{aligned}\tag{6}$$

where Ric denotes the Ricci curvature tensor whose definition can be found in Appendix A. The purpose of Ricci flow is to prove Thurston's Geometrization Conjecture and Poincaré Conjecture, which is to evolve the metric towards certain geometric structures and topological properties (Sheridan and Rubinstein, 2006).

Definition 3 (Sheridan and Rubinstein, 2006) *The Ricci flow is **strongly parabolic** if there exists $\delta > 0$ such that for all covectors $\varphi \neq 0$ and all (symmetric ⁵) $h_{ij} \neq 0$, the principal symbol of the differential operator $-2 \operatorname{Ric}$ satisfies*

$$[-2 \operatorname{Ric}](\varphi)(h)_{ij}h^{ij} = g^{pq}(\varphi_p\varphi_q h_{ij} + \varphi_i\varphi_j h_{pq} - \varphi_q\varphi_i h_{jp} - \varphi_q\varphi_j h_{ip})h^{ij} > \delta\varphi_k\varphi^k h_{rs}h^{rs}.$$

Theorem 4 *When $u(t) : \mathcal{M} \times [0, T] \rightarrow \mathcal{E}$ is a time-dependent section of the vector bundle \mathcal{E} where \mathcal{M} is a Riemannian manifold, if the system of the Ricci flow is strongly parabolic at u_0 where $u_0 = u(0) : \mathcal{M} \rightarrow \mathcal{E}$, then there exists a solution on the time interval $[0, T)$, and the solution is unique.*

Proof The proofs can be found in (Ladyzhenskaia et al., 1988). ■

Combined with Definition 3 and Theorem 4, one knows whether there exists a unique solution of Ricci flow for a short time by checking whether it is strongly parabolic. However, if we choose $h_{ij} = \varphi_i\varphi_j$, it is clear that the left hand side of the inequality in Definition 3 is 0, thus the inequality can not hold. Since the inequality can not always be satisfied, Ricci flow is not strongly parabolic, which makes us unable to prove the existence of the solution based on Theorem 4. Now, it is possible to understand which parts have an impact on its non-parabolic nature by the linearization of the Ricci curvature tensor.

Lemma 5 *The linearization of $-2 \operatorname{Ric}$ can be rewritten as ⁶*

$$\begin{aligned}D[-2 \operatorname{Ric}](h)_{ij} &= g^{pq}\nabla_p\nabla_q h_{ij} + \nabla_i V_j + \nabla_j V_i + O(h_{ij}) \\ \text{where } V_i &= g^{pq}\left(\frac{1}{2}\nabla_i h_{pq} - \nabla_q h_{pi}\right).\end{aligned}\tag{7}$$

Proof The proofs can be found in Appendix C.1. ■

By carefully observing the above equation, the impact on the non-parabolic of Ricci flow comes from the terms V_i and V_j (Sheridan and Rubinstein, 2006), instead of the

5. The differential operator $-2 \operatorname{Ric}$ always acts on the Riemannian metric, and the metric is always symmetric based on Definition 2. Hence, h_{ij} is required to be symmetric.

6. In this paper, we use the Einstein summation convention (for example, $(AB)_i^j = A_i^k B_k^j$). When the same index appears twice in one term, once as an upper index and the other time as a lower index, summation is automatically taken over this index even without the summation symbol.

term $g^{pq}\nabla_p\nabla_q h_{ij}$. On the other hand, the term $O(h_{ij})$ will have no contributions to the principal symbol of -2Ric , so we can ignore it in this problem. Using a time-dependent diffeomorphism $\varphi(t) : \mathcal{M} \rightarrow \mathcal{M}$ (with $\varphi(0) = \text{id}$), the pullback metrics $g(t)$ based on the pull back map φ^* can be expressed as

$$g(t) = \varphi^*(t)\bar{g}(t), \quad (8)$$

which satisfies the Ricci flow equation. Furthermore, the terms V_i and V_j can be reparameterized by choosing $\varphi(t)$ to form the Ricci-DeTurck flow that is strongly parabolic. The solution is followed by the DeTurck Trick (DeTurck, 1983) that has a time-dependent reparameterization of the manifold:

$$\begin{aligned} \frac{\partial}{\partial t}\bar{g}(t) &= -2\text{Ric}(\bar{g}(t)) - \mathcal{L}_{\frac{\partial\varphi(t)}{\partial t}}\bar{g}(t) \\ \bar{g}(0) &= \bar{g}_0, \end{aligned} \quad (9)$$

See Appendix C.2 for details. Thus, the Ricci-DeTurck flow has a unique solution for a short time. For the long time behavior, please refer to Appendix C.3.

2.4 Literature

For the Riemannian n -dimensional manifold (\mathcal{M}^n, g) that is isometric to the Euclidean n -dimensional space (\mathbb{R}^n, δ) , Schnürer et al. (Schnürer et al., 2007) have showed the stability of Euclidean space under the Ricci flow for a small C^0 perturbation. Koch et al. (Koch and Lamm, 2012) have given the stability of the Euclidean space along with the Ricci flow in the L^∞ -norm. Moreover, for the decay of the L^∞ -norm on Euclidean space, Appleton (Appleton, 2018) has provided a proof using a different method.

For a Ricci-flat metric with small perturbations, Guenther et al. (Guenther et al., 2002) proved that such metrics would converge under Ricci flow. Considering the stability of integrable and closed Ricci-flat metrics, Sesum (Sesum, 2006) has proved that the convergence rate is exponential because the spectrum of the Lichnerowicz operator is discrete. Furthermore, Deruelle et al. (Deruelle and Kröncke, 2021) have proved that an asymptotically locally Euclidean Ricci-flat metric is dynamically stable under the Ricci flow, with the $L^2 \cap L^\infty$ perturbation on non-flat and non-compact Ricci-flat manifolds.

3. Neural Networks in LNE Manifolds

The aim of this section is to build a LNE manifold via the information geometry (Amari, 2016) such that paving the way for the introduction of Ricci flow. Specifically, we first introduce a convex function (Equation (14)) to derive the LNE divergence (Theorem 9) with the help of Bregman divergence (Definition 8), and then construct the LNE metric (Equation (16)) by introducing the LNE divergence into a neural networks. Consequently, the LNE metric then appears in the steepest descent gradient (Lemma 10) of the LNE manifold. Of course, the mirror descent algorithm (Beck and Teboulle, 2003) can also equivalently construct the relationship between divergences and gradients, but it lacks the geometric meaning (manifold and metric) that is exactly what we need.

3.1 Neural Network Manifold

A neural network is composed of a large number of neurons connected with each other. The set of all such networks forms a manifold, where the weights represented by the neuron connections can be regarded as the coordinate system.

For the $n \times n$ matrix, all such matrices form an n^2 -dimensional manifold. Specifically, the matrix forms the $n(n+1)/2$ -dimensional manifold, i.e., a submanifold embedded in the manifold of all the matrices when this matrix is symmetric and positive-definite (Sheridan and Rubinstein, 2006). Note that such a matrix is described as the metric in the geometry theory. Since symmetric and positive-definite matrices have many advantages, which lead to wide implementations in many fields, our method will also construct such symmetric and positive-definite matrices (metrics) in neural networks.

Remark 6 *Comparing straight lines in Euclidean space, geodesics are the straightest possible lines that we can draw in a Riemannian manifold. Given a geodesic, there exists a unique non-Euclidean coordinate system. Once the curved coordinate system is selected in a Riemannian manifold, the symmetric and positive-definite metric is also given based on Definition 2. That geometry-based metric can describe the properties of manifolds, such as curvature (Helgason, 2001).*

3.2 Euclidean Space and Divergence

From the viewpoint of the information geometry, the metric can be deduced by the divergence satisfying the certain criteria (Basseville, 2013), which is summarized as Definition 7. By considering two nearby points P and Q in a manifold \mathcal{M} where these two points are expressed in coordinates as ξ_P and ξ_Q (column vectors), then the divergence is defined as half the square of an infinitesimal distance ds^2 between two sufficiently close points:

$$D[\xi_P : \xi_P + d\xi] = \frac{1}{2} ds^2. \quad (10)$$

Definition 7 (Amari, 2016) $D[P : Q]$ is called a **divergence** when it satisfies the following criteria:

- (1) $D[P : Q] \geq 0$,
- (2) $D[P : Q] = 0$ when and only when $P = Q$,
- (3) When P and Q are sufficiently close, by denoting their coordinates by ξ_P and $\xi_Q = \xi_P + d\xi$ where $d\xi$ denotes a sufficiently small coordinate change, the Taylor expansion of the divergence can be written as

$$D[\xi_P : \xi_P + d\xi] = \frac{1}{2} \sum_{i,j} g_{ij}(\xi_P) d\xi_i d\xi_j + O(|d\xi|^3), \quad (11)$$

and metric g_{ij} is positive-definite, depending on ξ_P .

Using an orthonormal coordinate system in the Euclidean space, the Euclidean divergence is naturally defined as a half of the square of the Euclidean distance between two nearby points ξ and ξ'

$$D_E[\xi : \xi'] = \frac{1}{2} \sum_i (\xi_i - \xi'_i)^2. \quad (12)$$

The metric g_{ij} is the Euclidean metric δ_{ij} in this case, so that

$$ds^2 = 2D_E[\boldsymbol{\xi} : \boldsymbol{\xi} + d\boldsymbol{\xi}] = \sum_i (d\xi_i)^2 = \sum_{i,j} \delta_{ij} d\xi_i d\xi_j. \quad (13)$$

Obviously, the Euclidean divergence satisfies the criteria of divergence. Note that the Euclidean metric δ_{ij} is the identity matrix \mathbf{I} where we still retain the notation of metrics because of the representation habit in the geometry theory.

3.3 LNE Manifold and Divergence

Recall that ⁷, in general relativity (Wald, 2010), the complete Riemannian manifold (\mathcal{M}, g) that is endowed with a linearly nearly flat spacetime metric, is considered to solve the Newtonian limit by the linearized gravity. The form of this metric is $g_{ij} = \eta_{ij} + \gamma_{ij}$ where η_{ij} represents a flat Minkowski metric whose background is special relativity and γ_{ij} is smallness. In practice, this is an excellent theory of small gravitational perturbations when gravity is “weak”.

Similarly, we give a metric $g_{ij} = \delta_{ij} + \gamma_{ij}$ in Riemannian n -manifold (\mathcal{M}^n, g_0) where δ_{ij} represents a flat Euclidean metric. An adequate definition of “smallness” in this context is that the components of γ_{ij} are much smaller than 1 in the global inertial coordinate system of δ_{ij} . Therefore, we can systematically develop the LNE metric to cope with small perturbations.

3.3.1 CONVEX FUNCTION

In order to construct the LNE manifold endowed with the LNE metric in the neural network, according to Definition 7, we can introduce the divergence to obtain the expression of the LNE metric, similar to the relationship between Euclidean metric and divergence.

The premise of constructing a divergence is to find a suitable convex function. There are many applications for different convex functions in physics and optimization (Bubeck et al., 2015). Thus, we can introduce a nonlinear function $\phi(\boldsymbol{\xi})$ of coordinates $\boldsymbol{\xi}$ as the convex function with a certain geometric structure to satisfy the needs of constructing the LNE divergence. When considering a differentiable function, it is said to be convex if and only if its Hessian is positive-definite

$$H(\boldsymbol{\xi}) = \left(\frac{\partial^2}{\partial \xi_i \partial \xi_j} \phi(\boldsymbol{\xi}) \right).$$

By drawing a tangent hyperplane touching it at point $\boldsymbol{\xi}'$

$$z = \phi(\boldsymbol{\xi}') + (\boldsymbol{\xi} - \boldsymbol{\xi}') \nabla \phi(\boldsymbol{\xi}'),$$

we can evaluate the distance between the convex function $\phi(\boldsymbol{\xi})$ and tangent hyperplane z . The graph describing their relationship is shown in Figure 3, where z is the vertical axis of the graph. Geometrically, we propose a symmetrized convex function with the certain geometric structure:

$$\phi(\boldsymbol{\xi}) = \sum_i \frac{1}{\tau^2} \log \frac{1}{2} (\exp(\tau \xi_i) + \exp(-\tau \xi_i)) = \sum_i \frac{1}{\tau^2} \log (\cosh(\tau \xi_i)) \quad (14)$$

7. The link between the LNE manifold and general relativity can be found in Section 2.2.

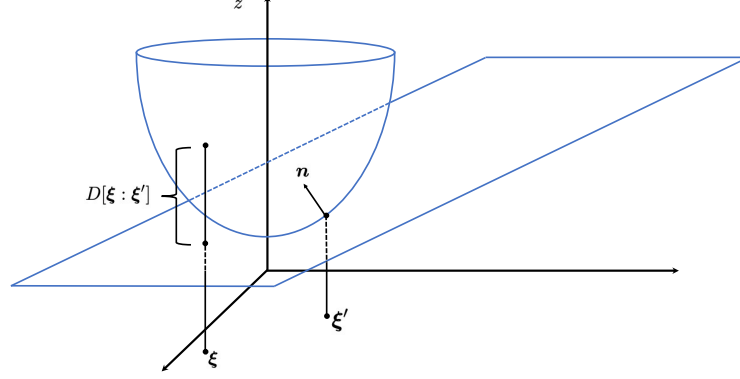


Figure 3: Convex function $z = \phi(\boldsymbol{\xi})$, its supporting hyperplane with normal vector $\mathbf{n} = \nabla\phi(\boldsymbol{\xi}')$ and divergence $D[\boldsymbol{\xi} : \boldsymbol{\xi}']$.

where τ is a constant parameter. Since ϕ is convex, the graph of ϕ is always above the hyperplane, touching it at $\boldsymbol{\xi}'$. With a supporting hyperplane of ϕ at $\boldsymbol{\xi}'$, we can deduce the LNE divergence through the Bregman divergence (Bregman, 1967).

3.3.2 LNE DIVERGENCE AND GRADIENT

Definition 8 (Bregman, 1967) The **Bregman divergence** $D_B[\boldsymbol{\xi} : \boldsymbol{\xi}']$ is defined as the difference between a convex function $\phi(\boldsymbol{\xi})$ and its tangent hyperplane $z = \phi(\boldsymbol{\xi}') + (\boldsymbol{\xi} - \boldsymbol{\xi}')\nabla\phi(\boldsymbol{\xi}')$, depending on the Taylor expansion at the point $\boldsymbol{\xi}'$:

$$D_B[\boldsymbol{\xi} : \boldsymbol{\xi}'] = \phi(\boldsymbol{\xi}) - \phi(\boldsymbol{\xi}') - (\boldsymbol{\xi} - \boldsymbol{\xi}')\nabla\phi(\boldsymbol{\xi}').$$

Theorem 9 By introducing a convex function ϕ defined by Equation (14) into Definition 8, the **LNE divergence** between two points $\boldsymbol{\xi}$ and $\boldsymbol{\xi}'$ yields

$$\begin{aligned} D_{LNE}[\boldsymbol{\xi}' : \boldsymbol{\xi}] &= \sum_i \left[\frac{1}{\tau^2} \log \frac{\cosh(\tau\xi'_i)}{\cosh(\tau\xi_i)} - \frac{1}{\tau} (\xi'_i - \xi_i) \tanh(\tau\xi_i) \right] \\ &\approx \frac{1}{2} \sum_{i,j} \delta_{ij} - \left[\tanh(\tau\xi) \tanh(\tau\xi)^\top \right]_{ij} d\xi_i d\xi_j. \end{aligned} \quad (15)$$

Proof The proofs can be found in Appendix F.1. ■

Comparing with Definition 7, we know that the LNE divergence satisfies the criteria of divergence, and the **LNE metric** corresponding to the LNE divergence is

$$\begin{aligned} g(\boldsymbol{\xi}) &= \delta_{ij} - \left[\tanh(\tau\xi) \tanh(\tau\xi)^\top \right]_{ij} \\ &= \begin{bmatrix} 1 - \tanh(\tau\xi_1) \tanh(\tau\xi_1) & \cdots & -\tanh(\tau\xi_1) \tanh(\tau\xi_n) \\ \vdots & \ddots & \vdots \\ -\tanh(\tau\xi_n) \tanh(\tau\xi_1) & \cdots & 1 - \tanh(\tau\xi_n) \tanh(\tau\xi_n) \end{bmatrix}. \end{aligned} \quad (16)$$

Based on Section 3.1, we are able to use the parameters of a neural network to construct the LNE metric (for a neural network, the coordinate $\boldsymbol{\xi}$ is the parameter vector). As a result, we can describe the neural network in the LNE manifold, as measured by the LNE divergence based on Theorem 9. Naturally, the steepest descent gradient in the LNE manifold is given by Lemma 10, which is similar to the natural gradient in Definition 1.

Lemma 10 *The steepest descent gradient measured by the LNE divergence is defined as*

$$\tilde{\partial}_{\boldsymbol{\xi}} = g(\boldsymbol{\xi})^{-1} \partial_{\boldsymbol{\xi}} = \left[\delta - \tanh(\tau \boldsymbol{\xi}) \tanh(\tau \boldsymbol{\xi})^\top \right]^{-1} \partial_{\boldsymbol{\xi}}. \quad (17)$$

Proof The proofs can be found in Appendix F.2. ■

Remark 11 *In fact, a divergence is derived from a convex function in the form of the Bregman divergence. By choosing different convex functions, for example, we can easily obtain the Euclidean divergence from the Bregman divergence, by defining the convex function: $\phi(\boldsymbol{\xi}) = 1/2 \sum_i \xi_i^2$ in a Euclidean space. Besides, given the convex function: $\phi(\boldsymbol{\xi}) = \sum_i p(\mathbf{x}, \xi_i) \log p(\mathbf{x}, \xi_i)$ where $\sum_i p(\mathbf{x}, \xi_i) = \sum_i p(\mathbf{x}, \xi'_i) = \int p(\mathbf{x}, \boldsymbol{\xi}) d\boldsymbol{\xi} = \int p(\mathbf{x}, \boldsymbol{\xi}') d\boldsymbol{\xi}' = 1$ is satisfied, the Bregman divergence is the same as the KL divergence.*

4. Evolution of LNE Manifolds under Ricci Flow

In this section, we will focus on LNE metrics under Ricci flow, and prove that the evolution of LNE manifolds can achieve good performances in terms of stability (short time and long time), i.e., the Ricci flow can exponentially decay the L^2 -norm perturbation to the LNE metric.

4.1 Analysis on LNE Metrics

To facilitate the handling of the metric perturbation, we have given the LNE metric in Equation (16), a special form of Ricci-flat metrics (Guenther et al., 2002; Deruelle and Kröncke, 2021), which means that the Ricci-flat metrics on noncompact manifolds are LNE. The full statement of the LNE metric is the linearly nearly Euclidean Ricci-flat metric ⁸ in Definition 12.

Definition 12 *(Deruelle and Kröncke, 2021) A complete Riemannian n -manifold (\mathcal{M}^n, g_0) is said to be LNE with one end of order $\iota > 0$ if there exists a compact set $K \subset \mathcal{M}$, a radius r , a point x in \mathcal{M} and a diffeomorphism satisfying $\phi : \mathcal{M} \setminus K \rightarrow (\mathbb{R}^n \setminus B(x, r))/SO(n)$. Note that $B(x, r)$ is the ball and $SO(n)$ is a finite group acting freely on $\mathbb{R}^n \setminus \{0\}$. Then*

$$\left| \partial^k (\phi_* \gamma) \right|_{\delta} = O(r^{-\iota-k}) \quad \forall k \geq 0 \quad (18)$$

holds on $(\mathbb{R}^n \setminus B(x, r))/SO(n)$. g_0 can be linearly decomposed into a form containing the Euclidean metric δ :

$$g_0 = \delta + \gamma. \quad (19)$$

⁸ In Equation (16), the form of the metric $g(\boldsymbol{\xi})$ constructed by the LNE divergence is consistent with the definition of LNE metrics, as long as we adjust parameter τ to satisfy Definition 12.

4.2 Short Time Convergence in the L^2 -norm

In this subsection, we consider the linear stability and integrability of the LNE manifold (\mathcal{M}^n, g_0) . Fortunately, similar to the previous proofs (Koiso, 1983; Besse, 2007), we can know that (\mathcal{M}^n, g_0) is integral and linearly stable based on Definition 27 and Definition 28.

Now, we introduce a metric perturbation for the Ricci–DeTurck flow based on Equation (9), i.e.,

$$\begin{aligned}\frac{\partial}{\partial t}\bar{g}(t) &= -2\text{Ric}(\bar{g}(t)) - \mathcal{L}_{\frac{\partial\varphi(t)}{\partial t}}\bar{g}(t) \\ \bar{g}(0) &= \bar{g}_0 + d\end{aligned}\tag{20}$$

where d is a metric perturbation deviated from the LNE metric. The main theorem is as follows, whose proof process is: Lemma 29 \rightarrow Lemma 30 \rightarrow Corollary 13. See Appendix D.

Corollary 13 *Let $(\mathcal{M}^n, \bar{g}_0)$ be the LNE n -manifold. For a Ricci–DeTurck flow $\bar{g}(t)$ on a maximal time interval $t \in [0, T)$, if it satisfies $\|\bar{g}(0) - \bar{g}_0\|_{L^\infty} < \epsilon$ where $\epsilon > 0$, then there exists a constant $C < \infty$ for $t \in (0, T)$. Then we further have*

$$\sup_{\mathcal{M}} \int_{\mathcal{M}} |d(t)|^2 \kappa^2 d\mu \leq e^{Ct} \sup_{\mathcal{M}} \int_{\mathcal{M}} |d(0)|^2 \kappa^2 d\mu.\tag{21}$$

Proof Based on Lemma 30, we obtain

$$\begin{aligned}\sup_{\mathcal{M}} \int_{\mathcal{M}} |d(t)|^2 \kappa^2 d\mu &\leq \sup_{\mathcal{M}} \int_{\mathcal{M}} |d(0)|^2 \kappa^2 d\mu \\ &\quad + N \left(C(\bar{g}_0) + \frac{2}{C_1 r^2} \right) \int_0^t \sup_{\mathcal{M}} \int_{\mathcal{M}} |d(s)|^2 \kappa^2 d\mu ds,\end{aligned}$$

where each ball of radius $2r$ on \mathcal{M} can be covered by N balls of radius r because $(\mathcal{M}^n, \bar{g}_0)$ is LNE. By the Gronwall inequality, we have

$$\sup_{\mathcal{M}} \int_{\mathcal{M}} |d(t)|^2 \kappa^2 d\mu \leq \exp \left(N \left(C(\bar{g}_0) + \frac{2}{C_1 r^2} \right) t \right) \sup_{\mathcal{M}} \int_{\mathcal{M}} |d(0)|^2 \kappa^2 d\mu.$$

Thus, for the LNE metric with the L^2 -norm perturbation, the Ricci–DeTurck flow in LNE manifolds is stable for a short time. \blacksquare

4.3 Long Time Stability in the L^2 -norm

In order to prove the long time stability of LNE metrics under Ricci–DeTurck flow, we need to construct $\bar{g}_0(t)$ that is a family of Ricci-flat reference metrics with $\frac{\partial}{\partial t}\bar{g}_0(t) = O((\bar{g}(t) - \bar{g}_0(t))^2)$. Let

$$\mathcal{F} = \left\{ \bar{g}(t) \in \mathcal{M}^n \mid 2\text{Ric}(\bar{g}(t)) + \mathcal{L}_{\frac{\partial\varphi(t)}{\partial t}}\bar{g}(t) = 0 \right\}$$

be the set of stationary points under the Ricci–DeTurck flow. Then, we are able to establish a manifold via an L^2 -neighbourhood \mathcal{U} of integral \bar{g}_0 in the space of metrics

$$\tilde{\mathcal{F}} = \mathcal{F} \cap \mathcal{U}.\tag{22}$$

For all $\bar{g} \in \tilde{\mathcal{F}}$, the terms $\text{Ric}(\bar{g}(t)) = 0$ and $\mathcal{L}_{\frac{\partial \varphi(t)}{\partial t}} \bar{g}(t) = 0$ hold individually, based on the previous work (Deruelle and Kröncke, 2021). In this way, $d(t) - d_0(t) = \bar{g}(t) - \bar{g}_0(t)$ holds because we write $d_0(t) = \bar{g}_0(t) - \bar{g}_0$.

The main theorem is as follows, whose proof process is: Corollary 13, Lemma 31, Lemma 29 and Corollary 33 \rightarrow Theorem 14 where Lemma 31 and Theorem 32 \rightarrow Corollary 33. See Appendix E.

Theorem 14 *Let $(\mathcal{M}^n, \bar{g}_0)$ be the LNE n -manifold which is linearly stable and integrable. For any metric $\bar{g}(t) \in \mathcal{B}_{L^2}(\bar{g}_0, \epsilon_2)$ where a constant $\epsilon_2 > 0$, there is a complete Ricci–DeTurck flow $(\mathcal{M}^n, \bar{g}(t))$ starting from $\bar{g}(t)$ converging to the LNE metric $\bar{g}(\infty) \in \mathcal{B}_{L^2}(\bar{g}_0, \epsilon_1)$ where ϵ_1 is a small enough constant.*

Proof By Lemma 29, we have a constant $\epsilon_2 > 0$ such that $d(t) \in \mathcal{B}_{L^2}(0, \epsilon_2)$ holds. By Lemma 31 (in the second step) and Corollary 33 (in the third step), we can obtain

$$\begin{aligned} \|d_0(T)\|_{L^2} &\leq C \int_1^T \left\| \frac{\partial}{\partial t} d_0(t) \right\|_{L^2} dt \\ &\leq C \int_1^T \|\nabla^{\bar{g}_0} (d(t) - d_0(t))\|_{L^2}^2 dt \\ &\leq C \|d(1) - d_0(1)\|_{L^2}^2 \leq C \|d(1)\|_{L^2}^2 \leq C \cdot (\epsilon_2)^2. \end{aligned}$$

Furthermore, we can obtain from the above formulas

$$\|d(T) - d_0(T)\|_{L^2} \leq \|d(1) - d_0(1)\|_{L^2} \leq C \cdot \epsilon_2.$$

By the triangle inequality, we get

$$\|d(T)\|_{L^2} \leq C \cdot (\epsilon_2)^2 + C \cdot \epsilon_2.$$

Followed by Corollary 13 and Lemma 31, T should be pushed further outward, i.e.,

$$\limsup_{t \rightarrow +\infty} \left\| \frac{\partial}{\partial t} d_0(t) \right\|_{L^2} \leq \limsup_{t \rightarrow +\infty} \|\nabla^{\bar{g}_0} (d(t) - d_0(t))\|_{L^2}^2 = 0.$$

Thus, $\bar{g}(t)$ will converge to $\bar{g}(\infty) = \bar{g}_0 + d_0(\infty)$ as t approaches $+\infty$ based on the elliptic regularity. In other words, $d(t) - d_0(t)$ will converge to 0 as t goes to $+\infty$ w.r.t. all Sobolev norms (Minerbe, 2009),

$$\lim_{t \rightarrow +\infty} \|d(t) - d_0(t)\|_{L^2} \leq \lim_{t \rightarrow +\infty} C \|\nabla^{\bar{g}_0} (d(t) - d_0(t))\|_{L^2} = 0.$$

We now conclude a result that any Ricci–DeTurck flow that starting close to the LNE metric exists for all time, and the Ricci–DeTurck flow will converge to the LNE metric, i.e., the L^2 -norm perturbation of the LNE metric can be dynamically decayed by the Ricci–DeTurck flow. ■

Thus, the Theorem 14 proves that LNE metrics can achieve good performances in terms of stability under the Ricci–DeTurck flow. Based on (Sesum, 2006), we further yields $|\bar{g}(t) - \bar{g}_0(\infty)| < Ce^{-\epsilon_2 t}$ such that the metric perturbation exponentially converges.

5. Discretized Neural Networks in LNE Manifolds

Up to now, we have theoretically solved the problem of gradient mismatch. Specifically, we have completed the construction of LNE manifolds for neural networks in Section 3 and decayed the metric perturbation in LNE manifolds in Section 4.

However, based on Lemma 10, there is the inverse of the LNE metric for the steepest descent gradient in the LNE manifold, which makes it difficult to be calculated in practice. Therefore, in this section, our aim is to approximate the inverse of the LNE metric, and further obtain the approximated gradient in the LNE manifold, that leads to the practical algorithm for training DNNs in the LNE manifold.

5.1 Gradient Computation in Discretized Neural Networks

Recall that Courbariaux et al. (2016) applied STE to binarized neural networks, whose form is given in Equation (1). Then, Zhou et al. (2016) applied STE to arbitrary bit-width discretized neural networks. Similarly, the generalization of STE in discretized neural networks yields

$$\frac{\partial L}{\partial \mathbf{w}} = \frac{\partial L}{\partial Q(\mathbf{w})} \cdot \mathbb{I}. \quad (23)$$

There is still a contradiction to be solved before the LNE manifold is introduced into the DNN. Based on Lemma 10, the LNE manifold is defined on the parameter $\boldsymbol{\xi}$ of all layers in a neural network. But, the gradient in back-propagation is defined layer-by-layer, i.e., on the weight \mathbf{w} of each layer, which causes that the gradient update can not be associated with the LNE manifold. Fortunately, the LNE manifold can be layer-by-layer redefined by replacing $\boldsymbol{\xi}$ with \mathbf{w} , which is equivalent to defining the LNE manifold for each layer. And on the basis of Lemma 10, the steepest descent gradient is rewritten as

$$\tilde{\partial}_{\mathbf{w}} = g^{-1}(\mathbf{w})\partial_{\mathbf{w}} = \left[\delta - \tanh(\tau\mathbf{w}) \tanh(\tau\mathbf{w})^{\top} \right]^{-1} \partial_{\mathbf{w}}, \quad (24)$$

which can be used for the gradient computation in DNNs, i.e.,

$$\frac{\tilde{\partial} L}{\tilde{\partial} \mathbf{w}} = \left[\delta - \tanh(\tau\mathbf{w}) \tanh(\tau\mathbf{w})^{\top} \right]^{-1} \frac{\partial L}{\partial Q(\mathbf{w})}. \quad (25)$$

When this form of the gradient is proposed, it means that we are in the framework of solving the problem of gradient mismatch, similar to Equation (5). Note that the metric at this time is layer-by-layer LNE. On the other hand, gradient computation involves the inverse of the LNE metric, which greatly consumes computing resources. Hence, we propose two methods for approximating the gradient of DNNs in LNE manifolds: weak approximation and strong approximation, respectively. The approximated gradient is defined as the direction in parameter space that gives the largest change in the objective per unit of change along the layer-by-layer LNE manifold.

5.2 Strong Approximation

For the $n \times n$ symmetric metric $g(\mathbf{w})$, it can be decomposed in terms of the combination of entries P and A , where P is the entries made up of the elements of the lower triangular

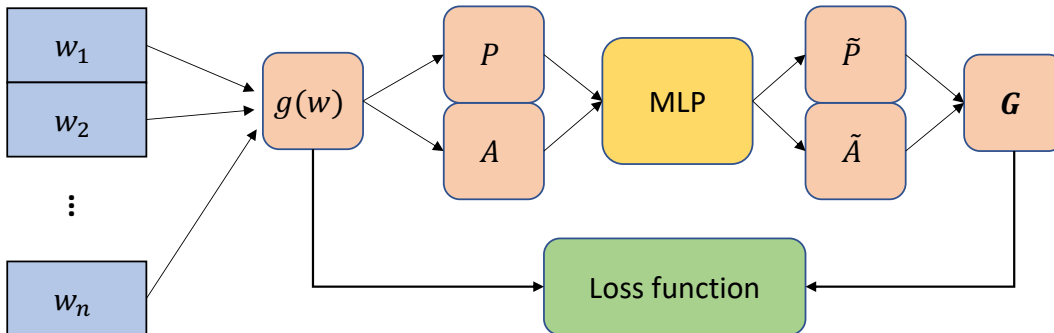


Figure 4: Flow chart of strong approximation of $g^{-1}(\mathbf{w})$. The new entries \tilde{P} and \tilde{A} produced by neural network form a matrix \mathbf{G} , which will multiply by the metric $g(\mathbf{w})$. As the loss function defined by Equation (26) decreases, the matrix \mathbf{G} can be used to approximate the inverse of the metric $g(\mathbf{w})$.

matrix that contains $n(n-1)/2$ real parameters and A is the entries made up of the elements of the diagonal matrix that contains n real parameters.

Our aim is to approximate the inverse of the LNE metric, and further approximate the gradient in Equation (25). Based on the universal approximation theorem (Cybenko, 1989; Hornik, 1991), a continuous function on compact subsets can be approximated by a neural network with a single hidden layer, and a finite number of neurons (Jejjala et al., 2020). Inspired by this, we introduce a multi-layer perceptron (MLP) neural network, as shown in Figure 4, to minimize the loss function

$$\tilde{L} = \|\mathbf{I} - g(\mathbf{w})\mathbf{G}\|^2, \tag{26}$$

such that the strong approximation of the inverse of the LNE metric is presented.

5.3 Weak Approximation

Of course, we can also approximate the inverse of the LNE metric by bypassing the introduction of the additional neural networks.

Definition 15 (Bhatia, 2013) For $\mathbf{A} \in \mathcal{R}^{n \times n}$, \mathbf{A} is called **diagonally dominant** when it satisfies

$$|a_{ii}| > \sum_{j=1, j \neq i}^n |a_{ij}|, \quad i = 1, 2, \dots, n.$$

Definition 16 (Bhatia, 2013) If $\mathbf{A} \in \mathcal{R}^{n \times n}$ is a diagonally dominant matrix, then \mathbf{A} is a **nonsingular matrix** together, i.e., \mathbf{A}^{-1} exists.

Considering the properties of the LNE metric, we can easily make $g^{-1}(\mathbf{w})$ satisfy Definition 15 by adjusting the parameter τ . And the existence of the inverse of the LNE metric can be guaranteed based on Definition 16. By placing a higher requirement, the LNE metric is diagonally dominant, which is a nice feature to facilitate the fast computation of the inverse.

Corollary 17 *Based on Definition 15 and Definition 16, the weak approximation of the gradient in the LNE manifold is defined as*

$$\tilde{\partial}_{\mathbf{w}} = \left[\delta - \tanh(\tau \mathbf{w}) \tanh(\tau \mathbf{w})^\top \right]^{-1} \partial_{\mathbf{w}} \approx \left[\delta + \tanh(\tau \mathbf{w}) \tanh(\tau \mathbf{w})^\top \right] \partial_{\mathbf{w}} \quad (27)$$

if the LNE metric is diagonally dominant.

Proof Considering the inverse of the LNE metric, due to the diagonally dominant property in Definition 15 and Definition 16, we can approximate $\left[\delta - \tanh(\tau \mathbf{w}) \tanh(\tau \mathbf{w})^\top \right]^{-1}$ by ignoring the fourth-order small quantity $\sum O(\rho_a \rho_b \rho_c \rho_d)$, i.e.,

$$\begin{aligned} & \left[\delta - \tanh(\tau \mathbf{w}) \tanh(\tau \mathbf{w})^\top \right]^{-1} \left[\delta + \tanh(\tau \mathbf{w}) \tanh(\tau \mathbf{w})^\top \right] \\ &= \begin{bmatrix} 1 - \rho_1 \rho_1 & -\rho_1 \rho_2 & \cdots \\ -\rho_2 \rho_1 & 1 - \rho_2 \rho_2 & \cdots \\ \vdots & \vdots & \ddots \end{bmatrix}^{-1} \begin{bmatrix} 1 + \rho_1 \rho_1 & \rho_1 \rho_2 & \cdots \\ \rho_2 \rho_1 & 1 + \rho_2 \rho_2 & \cdots \\ \vdots & \vdots & \ddots \end{bmatrix} \\ &= \begin{bmatrix} 1 - \sum O(\rho_a \rho_b \rho_c \rho_d) & \rho_1 \rho_2 - \rho_1 \rho_2 - \sum O(\rho_a \rho_b \rho_c \rho_d) & \cdots \\ -\rho_2 \rho_1 + \rho_2 \rho_1 - \sum O(\rho_a \rho_b \rho_c \rho_d) & 1 - \sum O(\rho_a \rho_b \rho_c \rho_d) & \cdots \\ \vdots & \vdots & \ddots \end{bmatrix} \approx \mathbf{I}. \end{aligned}$$

■

By now, we introduce the diagonally dominant property such that the weak approximation of the inverse of the LNE metric is presented.

5.4 Training

Consequently, based on the previous work (Courbariaux et al., 2016), we give the practical algorithm of DNNs in the LNE manifold. As shown in Algorithm 1, this algorithm is no differ from the general algorithm of DNNs, except for the Line 14. Recall that, in Figure 1, the general DNNs use STE to simply copy the gradient, i.e., $\tilde{\partial}_{\mathbf{W}_i} L = \partial_{\mathbf{W}_i} L$, but we match the gradient by introducing the LNE metric. Furthermore, we can practically compute this gradient in Line 14 via the strong approximation in Section 5.2 or the weak approximation in Section 5.3.

6. Ricci Flow Discretized Neural Networks

In this section, we propose Ricci flow discretized neural networks (RF-DNNs). When the Ricci flow is introduced, it implies that the background of DNNs we are discussing is the LNE manifold. Our aim is to provide a practical solution for the metric perturbation and

Algorithm 1 An algorithm for the training of DNNs in the LNE manifold. We represent the gradient in the LNE manifold as $\tilde{\partial}$. For brevity, we ignore the normalization operation (Ioffe and Szegedy, 2015; Ba et al., 2016).

Input: A minibatch of inputs and targets $(\mathbf{x} = \mathbf{a}_0, \mathbf{y})$, $\boldsymbol{\xi}$ mapped to $(\mathbf{W}_1, \mathbf{W}_2, \dots, \mathbf{W}_l)$, $\hat{\boldsymbol{\xi}}$ mapped to $(\hat{\mathbf{W}}_1, \hat{\mathbf{W}}_2, \dots, \hat{\mathbf{W}}_l)$, a nonlinear function f , a constant factor τ and a learning rate η .

Output: The updated discretized parameters $\hat{\boldsymbol{\xi}}$.

- 1: {Forward propagation}
- 2: **for** $i = 1; i \leq l; i++$ **do**
- 3: Discretize $\hat{\mathbf{W}}_i = Q(\mathbf{W}_i)$;
- 4: Compute $\mathbf{s}_i = \hat{\mathbf{W}}_i \hat{\mathbf{a}}_{i-1}$;
- 5: Discretize $\hat{\mathbf{a}}_i = Q(f \odot \mathbf{s}_i)$;
- 6: **end for**
- 7: {Loss derivative}
- 8: Compute $L = L(\mathbf{y}, \mathbf{z})$;
- 9: Compute $\partial_{\mathbf{a}_l} L = \left. \frac{\partial L(\mathbf{y}, \mathbf{z})}{\partial \mathbf{z}} \right|_{\mathbf{z}=\hat{\mathbf{a}}_l}$;
- 10: {Backward propagation}
- 11: **for** $i = l; i \geq 1; i--$ **do**
- 12: Compute $\partial_{\mathbf{s}_i} L = \partial_{\mathbf{a}_i} L \odot f'(\mathbf{s}_i)$;
- 13: Compute $\partial_{\hat{\mathbf{W}}_i} L = (\nabla_{\mathbf{s}_i} L) \hat{\mathbf{a}}_{i-1}^\top$;
- 14: Compute $\tilde{\partial}_{\mathbf{W}_i} L = g^{-1}(\mathbf{W}_i) \partial_{\hat{\mathbf{W}}_i} L$ based on Equation (25);
- 15: Compute $\partial_{\hat{\mathbf{a}}_{i-1}} L = \hat{\mathbf{W}}_i^\top (\partial_{\mathbf{s}_i} L)$;
- 16: **end for**
- 17: {The parameters update}
- 18: **for** $i = l; i \geq 1; i--$ **do**
- 19: Update $\mathbf{W}_i \leftarrow \mathbf{W}_i - \eta \cdot \tilde{\partial}_{\mathbf{W}_i} L$;
- 20: **end for**
- 21: Update $\hat{\boldsymbol{\xi}} = \left[\text{vec}(\hat{\mathbf{W}}_1)^\top, \text{vec}(\hat{\mathbf{W}}_2)^\top, \dots, \text{vec}(\hat{\mathbf{W}}_l)^\top \right]^\top$;

further for the problem of gradient mismatch. Therefore, we will focus on how to compute the discrete Ricci flow in practice rather than just staying on theoretical analysis.

To relate the Ricci flow to neural networks, we need to discretize the Ricci flow and choose a suitable coordinate system. For the left hand side of the Ricci flow, we have established the connection between the LNE metric and neural networks in Section 3. Note that we use the form of the LNE metric in the calculation, and such metrics at this time are with perturbations. For the right hand side of the Ricci flow, we need to compute the Ricci curvature tensor with the coordinate system. And this coordinate system is the key to linking the Ricci curvature and neural networks. Specifically, we define a method for calculating the Ricci curvature in such a way that the selection of coordinate systems is related to the input transformations, which implies that the Ricci curvature in neural networks reflects the effect of different input transformations on the parameter.

6.1 Ricci Curvature in Neural Networks

Now we consider the right hand side of the Ricci flow in Equation (6), the Ricci curvature tensor. According to Appendix A, it can be expressed as

$$\begin{aligned} -2 \operatorname{Ric}(g) &= -2R_{ikj}^i = 2R_{kij}^i \\ &= g^{ip} (\partial_i \partial_k g_{pj} - \partial_i \partial_j g_{pk} + \partial_p \partial_j g_{ik} + \partial_p \partial_k g_{ij}). \end{aligned} \quad (28)$$

In order to relate the Ricci curvature to neural networks, we define a method for calculating the Ricci curvature in such a way that the selection of coordinate systems is related to the input transformations. When the Ricci curvature is equal to zero, it means that different input transformations will not cause changes in the parameter (the metric is composed of the neural network parameter).

Inspired by the previous work (Kaul and Lall, 2019), we can treat the term ∂_i and ∂_p as changes for the translation and rotation of each input, respectively. In general, since the data augmentation in image classification tasks (He et al., 2016; Shorten and Khoshgoftaar, 2019) does not include the rotation, we consider the translation instead of the rotation by discarding the index p , i.e., $\partial_p(\partial_j g_{ik} + \partial_k g_{ij}) = 0$ for the fairness of ablation studies. Subsequently, $\partial_k g$ and $\partial_j g$ can be treated as changes for the row and column transformation of the input data w.r.t. the metric g , respectively. And the Ricci curvature can be rewritten as

$$-2 \operatorname{Ric}(g) = g^{ip} \partial_i (\partial_k g_{pj} - \partial_j g_{pk}). \quad (29)$$

Remark 18 *The choice of i and p is arbitrary (including k and j), and can even be other coordinate representations. Here, we just give it a specific geometric meaning by considering the characteristic of the image classification task.*

We replace partial derivatives with difference equations to discretize the Ricci curvature, i.e., $\partial_k g = (g|_{k1} - g|_{k2}) / (k1 - k2)$ and $\partial_j g = (g|_{j1} - g|_{j2}) / (j1 - j2)$ based on the input translation dimensions k and j , respectively. The Ricci curvature tensor can be further simplified as

$$-2 \operatorname{Ric}(g) = \frac{g|_{k1} - g|_{k2}}{k1 - k2} - \frac{g|_{j1} - g|_{j2}}{j1 - j2}. \quad (30)$$

In general, $(k1 - k2)$ and $(j1 - j2)$ are translations less than 4 pixels, which is consistent with data augmentation (He et al., 2016).

6.2 The Existence of Discrete Ricci Flow

Recall that we previously considered the Ricci-DeTurck flow instead of the Ricci flow as the solution of the Ricci flow does not always exist based on Section 2.3. However, we can not deal with the Ricci-DeTurck flow in DNNs because the Ricci-DeTurck flow depends on the choice of $\varphi(t)$. In contrast, the Ricci flow is relatively easy to be calculated. Then we can easily consider the Ricci flow in DNNs if we can ensure that the solution of Ricci flow exists.

To ensure the existence of the solution of Ricci flow in Equation (6), we require the tensor $-2\text{Ric}(g)$ will approach zero, as $\frac{\partial}{\partial t}g$ approaches zero⁹. Then we may achieve the goal ($-2\text{Ric}(g)$ approaches zero) by adding a regularization into the loss function to constrain the value of Ricci curvature in DNNs. Followed with Equation (30), we further present the regularization w.r.t. the metrics $g(t)$

$$g^{(t)}N = \left\| \frac{g^{(t)}|_{k1} - g^{(t)}|_{k2}}{k1 - k2} - \frac{g^{(t)}|_{j1} - g^{(t)}|_{j2}}{j1 - j2} \right\|_{L^2}^2, \quad (31)$$

where $g(t)$ is ϵ -close to the LNE metric g_0 based on Definition 34, which is the necessary condition for the evolution of Ricci flow. In other words, $g(t)$ is LNE metric with perturbations.

Combined with Definition 34, the upper bound of Equation (31) is estimated by

$$\begin{aligned} g^{(t)}N &\leq \left\| \frac{(1+\epsilon)^2 \cdot g_0|_{k1} - g_0|_{k2}}{(1+\epsilon)(k1 - k2)} - \frac{g_0|_{j1} - (1+\epsilon)^2 \cdot g_0|_{j2}}{(1+\epsilon)(j1 - j2)} \right\|_{L^2}^2 \\ &= \frac{1}{1+\epsilon} \left\| \frac{(1+\epsilon)^2 \cdot \gamma|_{k1} - \gamma|_{k2}}{k1 - k2} - \frac{\gamma|_{j1} - (1+\epsilon)^2 \cdot \gamma|_{j2}}{j1 - j2} + \frac{\epsilon^2 + 2\epsilon}{k1 - k2} \delta + \frac{\epsilon^2 + 2\epsilon}{j1 - j2} \delta \right\|_{L^2}^2, \end{aligned} \quad (32)$$

where the LNE metric g_0 can be decomposed into γ and δ based on Equation (19). And the lower bound of Equation (31) is estimated by

$$\begin{aligned} g^{(t)}N &\geq \left\| \frac{g_0|_{k1} - (1+\epsilon)^2 \cdot g_0|_{k2}}{(1+\epsilon)(k1 - k2)} - \frac{(1+\epsilon)^2 \cdot g_0|_{j1} - g_0|_{j2}}{(1+\epsilon)(j1 - j2)} \right\|_{L^2}^2 \\ &= \frac{1}{1+\epsilon} \left\| \frac{\gamma|_{k1} - (1+\epsilon)^2 \cdot \gamma|_{k2}}{k1 - k2} - \frac{(1+\epsilon)^2 \cdot \gamma|_{j1} - \gamma|_{j2}}{j1 - j2} - \frac{\epsilon^2 + 2\epsilon}{k1 - k2} \delta - \frac{\epsilon^2 + 2\epsilon}{j1 - j2} \delta \right\|_{L^2}^2. \end{aligned} \quad (33)$$

As the evolution of Ricci flow converges ($\epsilon \rightarrow 0$), the estimate of Equation (31) tends to be stable:

$$g^{(t)}N \xrightarrow{\text{Ricci flow}} N = \left\| \frac{\gamma|_{k1} - \gamma|_{k2}}{k1 - k2} - \frac{\gamma|_{j1} - \gamma|_{j2}}{j1 - j2} \right\|_{L^2}^2. \quad (34)$$

Therefore, we can also use the relaxed regularization N with the suitable coefficient α instead of the regularization $g^{(t)}N$. By constraining the relaxed regularization N in DNNs, the Ricci flow exists when $N \rightarrow 0$.

Remark 19 *In practice, we can compute $\gamma|_{k1}$, $\gamma|_{k2}$, $\gamma|_{j1}$ and $\gamma|_{j2}$ via 4 different translations of input data w.r.t. γ_{ij} where the metric satisfies $\gamma_{ij} = -\tanh(\tau\mathbf{w})\tanh(\tau\mathbf{w})^\top$.*

6.3 The Algorithm Design

Based on Equation (30), we present the expression of the discrete Ricci Flow

$$g(t+1)|_{k1} - g(t)|_{k1} = \frac{g^{(t)}|_{k1} - g^{(t)}|_{k2}}{k1 - k2} - \frac{g^{(t)}|_{j1} - g^{(t)}|_{j2}}{j1 - j2}. \quad (35)$$

9. There are two aspects to explain this reason. On the one hand, the convergence of the Ricci flow requires that the metric g converges. On the other hand, with the convergence of DNNs, the convergence of parameters also causes the metric g composed of parameters to converge.

Algorithm 2 An algorithm for the training our RF-DNNs in the LNE manifold. We define a parameter α for balancing the regularization. For brevity, we ignore the normalization operation (Ioffe and Szegedy, 2015; Ba et al., 2016).

Input: A minibatch of inputs and targets $(\mathbf{x} = \mathbf{a}_0, \mathbf{y}), \boldsymbol{\xi}$ mapped to $(\mathbf{W}_1, \mathbf{W}_2, \dots, \mathbf{W}_l)$, $\hat{\boldsymbol{\xi}}$ mapped to $(\hat{\mathbf{W}}_1, \hat{\mathbf{W}}_2, \dots, \hat{\mathbf{W}}_l)$, a nonlinear function f , a constant factor τ and a learning rate η .

Output: The updated discretized parameters $\hat{\boldsymbol{\xi}}$.

- 1: {Forward propagation}
 - 2: **for** $i = 1; i \leq l; i++$ **do**
 - 3: Compute $\hat{\mathbf{W}}_i = Q(\mathbf{W}_i)$;
 - 4: Compute $\mathbf{s}_i = \hat{\mathbf{W}}_i \hat{\mathbf{a}}_{i-1}$;
 - 5: Compute $\hat{\mathbf{a}}_i = Q(f \odot \mathbf{s}_i)$;
 - 6: **end for**
 - 7: Compute the relaxed regularization N based on Equation (34);
 - 8: {Loss derivative}
 - 9: Compute $L = L(\mathbf{y}, \mathbf{z}) + \alpha \cdot N$;
 - 10: Compute $\partial_{\mathbf{a}_i} L = \frac{\partial L(\mathbf{y}, \mathbf{z})}{\partial \mathbf{z}} \Big|_{\mathbf{z}=\hat{\mathbf{a}}_i}$;
 - 11: {Backward propagation}
 - 12: **for** $i = l; i \geq 1; i--$ **do**
 - 13: Compute $\partial_{\mathbf{s}_i} L = \partial_{\mathbf{a}_i} L \odot f'(\mathbf{s}_i)$;
 - 14: Compute the constraints $(\tilde{\mathbb{I}})$ of discrete Ricci flow based on Equation (36);
 - 15: Compute $\partial_{\hat{\mathbf{W}}_i} L = (\nabla_{\mathbf{s}_i} L) \hat{\mathbf{a}}_{i-1}^\top$;
 - 16: Compute $\tilde{\partial}_{\mathbf{W}_i} L = g^{-1}(\mathbf{W}_i) \partial_{\hat{\mathbf{W}}_i} L \cdot \tilde{\mathbb{I}}$ based on Equation (25);
 - 17: Compute $\partial_{\hat{\mathbf{a}}_{i-1}} L = \hat{\mathbf{W}}_i^\top (\partial_{\mathbf{s}_i} L)$;
 - 18: **end for**
 - 19: {The parameters update}
 - 20: **for** $i = l; i \geq 1; i--$ **do**
 - 21: Update $\mathbf{W}_i \leftarrow \mathbf{W}_i - \eta \cdot \tilde{\partial}_{\mathbf{W}_i} L$;
 - 22: **end for**
 - 23: Update $\hat{\boldsymbol{\xi}} = \left[\text{vec}(\hat{\mathbf{W}}_1)^\top, \text{vec}(\hat{\mathbf{W}}_2)^\top, \dots, \text{vec}(\hat{\mathbf{W}}_l)^\top \right]^\top$;
-

By applying the constraints of the discrete Ricci Flow in layer-by-layer LNE manifold, we can finally alleviate the problem of gradient mismatch. Since the background is the LNE manifold, we can construct the satisfied gradient on the basis of Equation (25). Note that, at this time, the metric is time-dependent under the Ricci flow, i.e., $g_{\mathbf{w}}(t)$.

By introducing a new indicator function $\tilde{\mathbb{I}}$ to represent the constraints of the discrete Ricci flow, we yield

$$\begin{aligned} \tilde{\partial}_{\mathbf{w}} L &= g_{\mathbf{w}}^{-1}(t) \partial_{Q(\mathbf{w})} \cdot \tilde{\mathbb{I}} \\ \text{where } \tilde{\mathbb{I}} &= \begin{cases} 1 & \text{if } \left| g(t+1)|_{k1} - g(t)|_{k1} - \frac{g(t)|_{k1} - g(t)|_{k2}}{k1 - k2} + \frac{g(t)|_{j1} - g(t)|_{j2}}{j1 - j2} \right| \leq \beta \\ 0 & \text{otherwise} \end{cases} \end{aligned} \quad (36)$$

where we define a small constant β , which implies that the cases less than or equal to β (rather than strictly equal to 0) all satisfy the discrete Ricci flow. The overall process is shown in Algorithm 2. Compared with Algorithm 1, we add the Line 7 and Line 14. In Line 7, we need to compute the relaxed regularization to ensure that the solution of discrete Ricci flow exists. On the other hand, in Line 14, we compute the constraints of discrete Ricci flow to alleviate the problem of gradient mismatch.

Remark 20 *In addition to using the discretized weight and activation, DNNs need to save the non-discretized weight and activation for gradient update. Note that the gradient of a DNN is non-discretized.*

7. Experiments

In this section, we design ablation studies to compare our RF-DNN¹⁰ trained from scratch with other STE methods. Furthermore, given a pre-trained model, we evaluate the performance of the RF-DNN in comparison with several representative training-based methods on classification benchmark datasets. All the experiments implemented in Python are conducted with PyTorch (Paszke et al., 2019). The hardware environment is conducted on a Workstation with an Intel(R) Xeon(R) Silver 4214 CPU(2.20 GHz), GeForce GTX 1080Ti GPU and 128GB RAM.

7.1 Experimental Settings

The two datasets used in our experiments are introduced as follows.

CIFAR datasets: There are two CIFAR benchmarks (Krizhevsky et al., 2009) consisting of natural color images with 32×32 pixels, respectively, 50k training and 10k test images, and we pick out 5k training images as a validation set from the training set. CIFAR-10 consists of images organized into 10 classes and CIFAR-100 into 100 classes. We adopt a standard data augmentation scheme (random corner cropping and random flipping) that is widely used for these two datasets. We normalize the images with the means of the channel and standard deviations in preprocessing.

ImageNet dataset: The ImageNet benchmark (Russakovsky et al., 2015) consists of 1.2 million high-resolution natural images, where the validation set contains 50k images. These images are organized into 1000 categories of the objects for training, which are resized to 224×224 pixels before fed into the network. In the next experiments, we report our single-crop evaluation results using top-1 and top-5 accuracies.

We specify the discrete function, the composition of which has a significant influence on the performance and computation of DNNs. Specifically, the discrete function is able to simplify the calculations which are also varied depending on the different discrete values, e.g., fixed-point multiplication, SHIFT operation (Elhoushi et al., 2019) and XNOR operation (Rastegari et al., 2016) etc.

We mark Q^1 as the 1-bit discrete function:

$$Q^1(\cdot) = \text{sign}(\cdot) = \{-1, +1\}. \quad (37)$$

10. In order to calculate the gradient conveniently, we use the weak approximation of the inverse of the LNE metric in all experiments.

Table 1: The experimental results on CIFAR10 with ResNet20/32/44. The accuracy of full-precision (FP) baseline is reported by (Chen et al., 2019).

Network	Forward	Backward	Test Acc (%)	FP Acc (%)
ResNet20	$\{-1,+1\}$	Dorefa	88.28±0.81	91.50
		MultiFCG	88.94±0.46	
		RF-DNN	89.83±0.23	
ResNet32	$\{-1,+1\}$	Dorefa	90.23±0.63	92.13
		MultiFCG	89.63±0.38	
		RF-DNN	90.75±0.19	
ResNet44	$\{-1,+1\}$	Dorefa	90.71±0.58	93.56
		MultiFCG	90.54±0.21	
		RF-DNN	91.63±0.11	

The k -bit, over 1-bit, discrete function can be marked as Q^k ,

$$Q^{k>1}(\cdot) = \frac{2}{2^k - 1} \text{round} \left[(2^k - 1) \left(\frac{\cdot}{2 \max|\cdot|} + \frac{1}{2} \right) \right] - 1 \quad (38)$$

where $\text{round}[\cdot]$ is the rounding function and $\max|\cdot|$ means to calculate the absolute value of the input first, and then find its maximum value. In this way, a DNN using discrete function $Q^1(\cdot)$ can be calculated with XNOR operation and using discrete function $Q^{k>1}(\cdot)$ can be calculated with fixed-point multiplication.

7.2 Ablation Studies with STE Methods

In order to illustrate the superiority of RF-DNN against the problem of gradient mismatch, we compare our RF-DNN with three other methods by training from scratch. In Table 1, Table 2 and Table 3, we mark $\{-1,+1\}$ in ‘**Forward**’, which indicates that the weights are binarized using Equation (37), i.e., -1 or $+1$, in the forward of DNNs. In the backward, the methods (Dorefa (Zhou et al., 2016), MultiFCG (Chen et al., 2019) and FCGrad (Chen et al., 2019)) use the different approximated gradients to update the weights. Here, we apply different ResNet models (He et al., 2016) to compare ablation studies.

The batch normalization with a batch size of 128 is used in the learning strategy, and Nesterov momentum of 0.9 (Dozat, 2016) is used in SGD optimization. For CIFAR, we set total training epochs as 200 and set a weight decay of 0.0005 where the learning rate is lowered by 10 times at epoch 80, 150, and 190, with the initial value of 0.1. For ImageNet, we set total training epochs as 100 and set the learning rate of each parameter group using a cosine annealing schedule with a weight decay of 0.0001. All experiments are conducted for 5 times, and the statistics of the last 10/5 epochs’ test accuracies are reported for a fair comparison. Note that we perform standard data augmentation and pre-processing on CIFAR and ImageNet datasets.

Table 2: The experimental results on CIFAR100 with ResNet56/110. The accuracy of full-precision (FP) baseline is reported by (Chen et al., 2019).

Network	Forward	Backward	Test Acc (%)	FP Acc (%)
ResNet56	{-1,+1}	Dorefa	66.71±2.32	71.22
		MultiFCG	66.58±0.37	
		FCGrad	66.56±0.35	
		RF-DNN	68.56±0.32	
ResNet110	{-1,+1}	Dorefa	68.15±0.50	72.54
		MultiFCG	68.27±0.14	
		FCGrad	68.74±0.36	
		RF-DNN	69.20±0.28	

Table 3: The experimental results on ImageNet with ResNet18. The accuracy of full-precision (FP) baseline is reported by (Chen et al., 2019).

Network	Forward	Backward	Test Top1/Top5 (%)	FP Top1/Top5 (%)
ResNet18	{-1,+1}	Dorefa	58.34±2.07/81.47±1.56	69.76/89.08
		MultiFCG	59.47±0.02/82.41±0.01	
		FCGrad	59.83±0.36/82.67±0.23	
		RF-DNN	60.83±0.41/83.54±0.18	

In Table 1, Table 2 and Table 3, we use the same the discrete function $Q^1(\cdot)$, parameter setting and optimizer for fairness in the forward. The only difference is the gradient in the backward propagation. The performance in various models and datasets shows that our RF-DNN has significant improvement over other STE methods. The average results of multiple experiments are better than that of other methods, which may benefit from the alleviation of the gradient mismatch to make the loss function of DNNs more fully descended. In addition, the minor variances show that our training method is relatively stable, which also confirms our point of view.

7.3 Convergence and Stability Analysis

Based on the above ablation studies, we compare the convergence and stability of our RF-DNN and Dorefa during the training and test processes. As shown in Figure 5, the RF-DNN can achieve higher accuracies than Dorefa on CIFAR100 dataset, i.e., 1.25% higher on the training dataset with ResNet56, 1.85% higher on the test dataset with ResNet56, 1.97% higher on the training dataset with ResNet110 and 1.05% higher on the test dataset with ResNet110. In addition, it can be seen from the fluctuation of the test curves in Figure 5

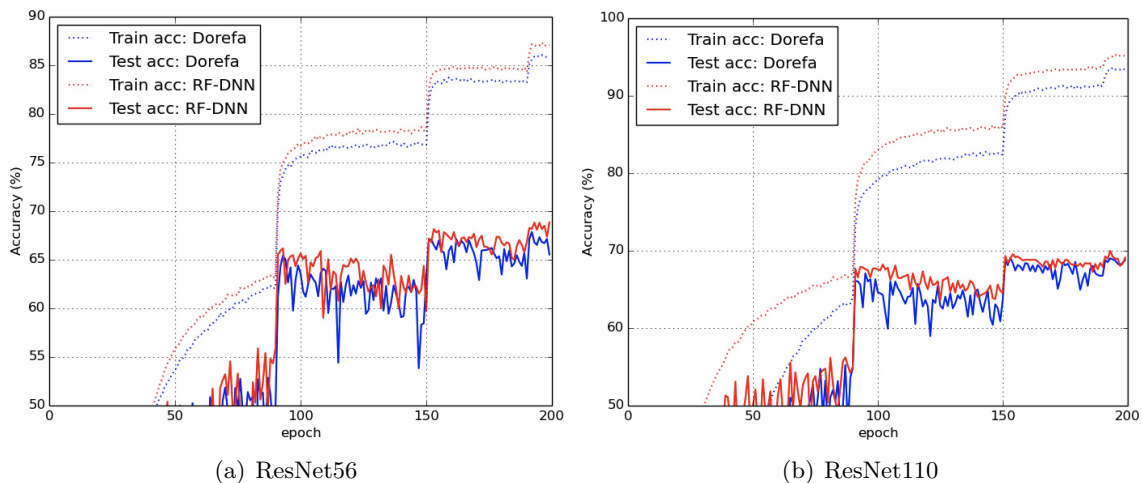


Figure 5: Training and test curves of ResNet56/110 on CIFAR100 compared between Dorefa and RF-DNN.

that the RF-DNN has a tremendous improvement compared with the Dorefa on the stability of training.

From the training curve, our method significantly outperforms Dorefa, of course, this needs to be combined with the test curve to explain the superiority of RF-DNN. From the test curve, the accuracy of our method is always higher than that of Dorefa, and the corresponding volatility has improved. The experimental results verify that our theoretical framework is an effective solution against the gradient mismatch, further improving the training performance of DNNs.

7.4 Training Time Analysis

In our hardware environment, we record the training time per iteration for our RF-DNN, MultiFCG, and Dorefa with the ResNet20 model in the CIFAR10 dataset. For each training iteration, our RF-DNN costs 35.34 seconds, MultiFCG costs 18.44 seconds, and Dorefa costs 17.81 seconds. Compared with MultiFCG and Dorefa, our RF-DNN costs more calculation time, and this part of the extra time mainly comes from solving the constraints of the Ricci flow. Although the training time of our RF-DNN is longer, it is acceptable compared to the improvement brought by our method. And our method also has room for parallel optimization, but it is out of the scope of this paper.

7.5 Comparisons with Training-based Methods

In this experiment, based on a full-precision pre-trained model, we compare the RF-DNN with several state-of-the-art DNNs, e.g., DeepShift (Elhoushi et al., 2019), QN (Yang et al., 2019), ADMM (Leng et al., 2018), MetaQuant (Chen et al., 2019), INT8 (Zhu et al., 2020), SR+DR (Gysel et al., 2018), ELQ (Zhou et al., 2018), MD (Ajanthan et al., 2021) and RQ (Louizos et al., 2019), under the same bit width using Equation (37) or Equation (38).

Table 4: The classification accuracy results on ImageNet and comparison with other training-based methods, with AlexNet (Krizhevsky et al., 2012), ResNet18, ResNet50 and MobileNet (Howard et al., 2017). Note that the accuracy of full-precision baseline is reported by (Elhoushi et al., 2019).

Method	W	A	Top-1		Top-5	
			Accuracy	Gap	Accuracy	Gap
AlexNet (Original)	32	32	56.52%	-	79.07%	-
RF-DNN (ours)	6	32	56.39%	-0.13%	78.78%	-0.29%
DeepShift (Elhoushi et al., 2019)	6	32	54.97%	-1.55%	78.26%	-0.81%
ResNet18 (Original)	32	32	69.76%	-	89.08%	-
RF-DNN (ours)	1	32	67.05%	-2.71%	88.09%	-0.99%
MD (Ajanthan et al., 2021)	1	32	66.78%	-2.98%	87.01%	-2.07%
ELQ (Zhou et al., 2018)	1	32	66.21%	-3.55%	86.43%	-2.65%
ADMM (Leng et al., 2018)	1	32	64.80%	-4.96%	86.20%	-2.88%
QN (Yang et al., 2019)	1	32	66.50%	-3.26%	87.30%	-1.78%
MetaQuant (Chen et al., 2019)	1	32	63.44%	-6.32%	84.77%	-4.31%
RF-DNN (ours)	4	4	66.75%	-3.01%	87.02%	-2.06%
RQ ST (Louizos et al., 2019)	4	4	62.46%	-7.30%	84.78%	-4.30%
ResNet50 (Original)	32	32	76.13%	-	92.86%	-
RF-DNN (ours)	8	8	76.07%	-0.06%	92.87%	+0.01%
INT8 (Zhu et al., 2020)	8	8	75.87%	-0.26%	-	-
MobileNet (Original)	32	32	70.61%	-	89.47%	-
RF-DNN (ours)	5	5	61.32%	-9.29%	84.08%	-5.39%
SR+DR (Gysel et al., 2018)	5	5	59.39%	-11.22%	82.35%	-7.12%
RQ ST (Louizos et al., 2019)	5	5	56.85%	-13.76%	80.35%	-9.12%
RF-DNN (ours)	8	8	70.76%	+0.15%	89.54%	+0.07%
RQ (Louizos et al., 2019)	8	8	70.43%	-0.18%	89.42%	-0.05%

Note that **W** and **A** represent the bit width of weights and activations respectively in Table 4. Consequently, the experimental results show that our RF-DNN is able to achieve better performance than other recent state-of-the-art training-based methods, which seems to benefit from our effective solution of the gradient mismatch.

8. Conclusion and Future Work

This paper studies discretized neural networks (DNNs), where the weights can only take low-precision discrete values, as well as the activations. This makes DNNs' memory footprint

very light compared to full-precision floating point networks. However, it makes their training difficult: to maintain discrete weights, the gradient w.r.t. discrete weights is in general approximated with the Straight-Through Estimator (STE), which causes the update weight to differ from the gradient w.r.t. continuous weights (*gradient mismatch*).

We propose an analysis of the gradient mismatch phenomenon through the lens of duality theory. This mismatch is then viewed as a metric perturbation in a Riemannian manifold. In theory, we construct the LNE manifold for neural networks, based on the information geometry, such that forming the background to deal with a metric perturbation. By proving the stability of LNE metrics with the L^2 -norm perturbation under the Ricci-DeTurck flow, we subsequently introduce the Ricci flow Discretized Neural Network (RF-DNN) in practice by using the constraints of the discrete Ricci flow in the LNE manifold to alleviate the metric perturbation. Experimentally, our RF-DNN achieves improvements in both the stability and performance of DNNs.

In this paper, information geometry is a very important part of combining the geometric tool (Ricci flow) and neural networks. Our future research will continue to explore the connection between neural networks and manifolds and aim to introduce geometric ideas to solve practical problems in machine learning.

Acknowledgments

We thank all reviewers and the editor for excellent contributions.

Appendix A. Differential Geometry

1. Riemann curvature tensor (Rm) is a (1,3)-tensor defined for a 1-form ω :

$$R_{ijk}^l \omega_l = \nabla_i \nabla_j \omega_k - \nabla_j \nabla_i \omega_k$$

where the covariant derivative of F satisfies

$$\nabla_p F_{i_1 \dots i_k}^{j_1 \dots j_l} = \partial_p F_{i_1 \dots i_k}^{j_1 \dots j_l} + \sum_{s=1}^l F_{i_1 \dots i_k}^{j_1 \dots q \dots j_l} \Gamma_{pq}^{j_s} - \sum_{s=1}^k F_{i_1 \dots q \dots i_k}^{j_1 \dots j_l} \Gamma_{pi_s}^q.$$

In particular, coordinate form of the Riemann curvature tensor is:

$$R_{ijk}^l = \partial_i \Gamma_{jk}^l - \partial_j \Gamma_{ik}^l + \Gamma_{jk}^p \Gamma_{ip}^l - \Gamma_{ik}^p \Gamma_{jp}^l.$$

2. Christoffel symbol in terms of an ordinary derivative operator is:

$$\Gamma_{ij}^k = \frac{1}{2} g^{kl} (\partial_i g_{jl} + \partial_j g_{il} - \partial_l g_{ij}).$$

3. Ricci curvature tensor (Ric) is a (0,2)-tensor:

$$R_{ij} = R_{pij}^p.$$

4. Scalar curvature is the trace of the Ricci curvature tensor:

$$R = g^{ij} R_{ij}.$$

5. Lie derivative of F in the direction $\frac{d\varphi(t)}{dt}$:

$$\mathcal{L}_{\frac{d\varphi(t)}{dt}} F = \left(\frac{d}{dt} \varphi^*(t) F \right)_{t=0}$$

where $\varphi(t) : \mathcal{M} \rightarrow \mathcal{M}$ for $t \in (-\epsilon, \epsilon)$ is a time-dependent diffeomorphism of \mathcal{M} to \mathcal{M} .

Appendix B. Notation

For clarity of definitions in this paper, we list the important notations as shown in Table 5.

Appendix C. Proof for the Ricci Flow

C.1 Proof for Lemma 5

Theorem 21 *The linearization of the Ricci curvature tensor is given by*

$$D[\text{Ric}](h)_{ij} = -\frac{1}{2} g^{pq} (\nabla_p \nabla_q h_{ij} + \nabla_i \nabla_j h_{pq} - \nabla_q \nabla_i h_{jp} - \nabla_q \nabla_j h_{ip}).$$

Proof Based on Appendix A, we have

$$\nabla_q \nabla_i h_{jp} = \nabla_i \nabla_q h_{jp} - R_{qij}^r h_{rp} - R_{qip}^r h_{jm}.$$

Table 5: Definitions of notations

\mathbf{W}_i :	weight matrix for the i -th layer	$\hat{\mathbf{W}}_i$:	discretized weight matrix for the i -th layer
\mathbf{a}_i :	activation vector for the i -th layer	$\hat{\mathbf{a}}_i$:	discretized activation vector for the i -th layer
$\boldsymbol{\xi}$:	parameter vector	$\hat{\boldsymbol{\xi}}$:	discretized parameter vector
Q^1 :	1-bit discrete function	$Q^{k>1}$:	k-bit discrete function (over 1-bit)
δ :	Euclidean metric (identity matrix)	g or $g(t)$:	the pullback metrics under Ricci flow
g_0 :	LNE metric under Ricci flow	$g(0)$:	initial metric under Ricci flow
g_x :	a metric for any point $x \in \mathcal{M}$	\bar{g} or $\bar{g}(t)$:	metrics under Ricci-DeTurck flow
$\bar{g}(0)$:	an initial metric under Ricci-DeTurck flow	\bar{g}_0 :	LNE metric under Ricci-DeTurck flow
$\bar{g}_0(t)$:	the family of Ricci-flat metrics	$d(t)$:	the time-dependent difference
$d(0)$:	the initial perturbation	L :	loss function
L_{g_0} :	Lichnerowicz operator	L^2 or L^∞ :	norm
∂ :	partial derivative	∇ :	covariant derivative
\mathcal{L} :	Lie derivative	Δ_{g_0} :	the Laplacian
Rm:	Riemann curvature tensor	Rm_x :	Riemann curvature tensor for any point $x \in \mathcal{M}$
Ric:	Ricci curvature tensor	D :	divergence
φ^* :	pull back map	ϕ_* :	push forward map
$D[\text{Ric}]$:	the linearization of the Ricci curvature tensor	$\mathcal{B}_{L^2}(\bar{g}_0, \epsilon)$:	the ϵ -ball with respect to the L^2 -norm induced by \bar{g}_0 and centred at \bar{g}_0
$B(x, r)$:	the ball with a radius r and a point $x \in \mathcal{M}$		

Combining with Definition 21, we can obtain the deformation equation because of $\nabla_k g_{ij} = 0$,

$$\begin{aligned}
 D[-2\text{Ric}](h)_{ij} &= g^{pq} \nabla_p \nabla_q h_{ij} + \nabla_i \left(\frac{1}{2} \nabla_j h_{pq} - \nabla_q h_{jp} \right) + \nabla_j \left(\frac{1}{2} \nabla_i h_{pq} - \nabla_q h_{ip} \right) + O(h_{ij}) \\
 &= g^{pq} \nabla_p \nabla_q h_{ij} + \nabla_i V_j + \nabla_j V_i + O(h_{ij}).
 \end{aligned}$$

■

C.2 Description of the DeTurck Trick

Based on the chain rule for the Lie derivative in Appendix A, we can calculate

$$\begin{aligned}
 \frac{\partial}{\partial t}g(t) &= \frac{\partial(\varphi^*(t)\bar{g}(t))}{\partial t} \\
 &= \left(\frac{\partial(\varphi^*(t+\tau)\bar{g}(t+\tau))}{\partial \tau} \right)_{\tau=0} \\
 &= \left(\varphi^*(t) \frac{\partial \bar{g}(t+\tau)}{\partial \tau} \right)_{\tau=0} + \left(\frac{\partial(\varphi^*(t+\tau)\bar{g}(t))}{\partial \tau} \right)_{\tau=0} \\
 &= \varphi^*(t) \frac{\partial}{\partial t} \bar{g}(t) + \varphi^*(t) \mathcal{L}_{\frac{\partial \varphi(t)}{\partial t}} \bar{g}(t)
 \end{aligned}$$

where $\frac{\partial \varphi(t)}{\partial t}$ is equal to $V(t)$ (Sheridan and Rubinstein, 2006). With the help of Equation (6), we have the following expression for the pullback metric $g(t)$

$$\frac{\partial}{\partial t}g(t) = \varphi^*(t) \frac{\partial}{\partial t} \bar{g}(t) + \varphi^*(t) \mathcal{L}_{\frac{\partial \varphi(t)}{\partial t}} \bar{g}(t) = -2 \operatorname{Ric}(\varphi^*(t)\bar{g}(t)) = -2\varphi^*(t) \operatorname{Ric}(\bar{g}(t)). \quad (39)$$

The diffeomorphism invariance of the Ricci curvature tensor is used in the last step. The above equation is equivalent to

$$\frac{\partial}{\partial t} \bar{g}(t) = -2 \operatorname{Ric}(\bar{g}(t)) - \mathcal{L}_{\frac{\partial \varphi(t)}{\partial t}} \bar{g}(t).$$

Based on Definition 22, we further yield

$$\frac{\partial}{\partial t} \bar{g}(t) = -2 \operatorname{Ric}(\bar{g}(t)) - \nabla_i V_j - \nabla_j V_i.$$

Definition 22 (Sheridan and Rubinstein, 2006) *On a Riemannian manifold (\mathcal{M}, g) , we have*

$$(\mathcal{L}_X g)_{ij} = \nabla_i X_j + \nabla_j X_i,$$

where ∇ denotes the Levi-Civita connection of the metric g , for any vector field X .

C.3 Curvature Explosion at Singularity

In general, we present the behavior of Ricci flow in finite time and show that the evolution of the curvature is close to divergence. The core demonstration is followed with Theorem 26.

Theorem 23 *Given a smooth Riemannian metric g_0 on a closed manifold \mathcal{M} , there exists a maximal time interval $[0, T)$ such that a solution $g(t)$ of the Ricci flow, with $g(0) = g_0$, exists and is smooth on $[0, T)$, and this solution is unique.*

Proof The proofs can be found in (Sheridan and Rubinstein, 2006). ■

Theorem 24 *Let \mathcal{M} be a closed manifold and $g(t)$ a smooth time-dependent metric on \mathcal{M} , defined for $t \in [0, T)$. If there exists a constant $C < \infty$ for all $x \in \mathcal{M}$ such that*

$$\int_0^T \left| \frac{\partial}{\partial t} g_x(t) \right|_{g(t)} dt \leq C, \quad (40)$$

then the metrics $g(t)$ converge uniformly as t approaches T to a continuous metric $g(T)$ that is uniformly equivalent to $g(0)$ and satisfies

$$e^{-C} g_x(0) \leq g_x(T) \leq e^C g_x(0). \quad (41)$$

Proof Considering any $x \in \mathcal{M}$, $t_0 \in [0, T)$, $V \in T_x \mathcal{M}$, we have

$$\begin{aligned} \left| \log \left(\frac{g_x(t_0)(V, V)}{g_x(0)(V, V)} \right) \right| &= \left| \int_0^{t_0} \frac{\partial}{\partial t} [\log g_x(t)(V, V)] dt \right| \\ &= \left| \int_0^{t_0} \frac{\frac{\partial}{\partial t} g_x(t)(V, V)}{g_x(t)(V, V)} dt \right| \\ &\leq \int_0^{t_0} \left| \frac{\partial}{\partial t} g_x(t) \left(\frac{V}{|V|_{g(t)}}, \frac{V}{|V|_{g(t)}} \right) \right| dt \\ &\leq \int_0^{t_0} \left| \frac{\partial}{\partial t} g_x(t) \right|_{g(t)} dt \\ &\leq C. \end{aligned}$$

By exponentiating both sides of the above inequality, we have

$$e^{-C} g_x(0)(V, V) \leq g_x(t_0)(V, V) \leq e^C g_x(0)(V, V).$$

This inequality can be rewritten as

$$e^{-C} g_x(0) \leq g_x(t_0) \leq e^C g_x(0)$$

because it holds for any V . Thus, the metrics $g(t)$ are uniformly equivalent to $g(0)$.

Consequently, we have the well-defined integral:

$$g_x(T) - g_x(0) = \int_0^T \frac{\partial}{\partial t} g_x(t) dt.$$

We can show that this integral is well-defined from two perspectives. Firstly, as long as the metrics are smooth, the integral exists. Secondly, the integral is absolutely integrable. Based on the norm inequality induced by $g(0)$, we can obtain

$$|g_x(T) - g_x(t)|_{g(0)} \leq \int_t^T \left| \frac{\partial}{\partial t} g_x(t) \right|_{g(0)} dt.$$

For each $x \in \mathcal{M}$, the above integral will approach zero as t approaches T . Since \mathcal{M} is compact, the metrics $g(t)$ converge uniformly to a continuous metric $g(T)$ which is uniformly equivalent to $g(0)$ on \mathcal{M} . Moreover, we can show that

$$e^{-C} g_x(0) \leq g_x(T) \leq e^C g_x(0).$$

■

Corollary 25 *Let $(\mathcal{M}, g(t))$ be a solution of the Ricci flow on a closed manifold. If $|\text{Rm}|_{g(t)}$ is bounded on a finite time $[0, T)$, then $g(t)$ converges uniformly as t approaches T to a continuous metric $g(T)$ which is uniformly equivalent to $g(0)$.*

Proof The bound on $|\text{Rm}|_{g(t)}$ implies one on $|\text{Ric}|_{g(t)}$. Based on Equation (6), we can extend the bound on $|\frac{\partial}{\partial t}g(t)|_{g(t)}$. Therefore, we obtain an integral of a bounded quantity over a finite interval is also bounded, by Theorem 24. ■

Theorem 26 *If g_0 is a smooth metric on a compact manifold \mathcal{M} , the Ricci flow with $g(0) = g_0$ has a unique solution $g(t)$ on a maximal time interval $t \in [0, T)$. If $T < \infty$, then*

$$\lim_{t \rightarrow T} \left(\sup_{x \in \mathcal{M}} |\text{Rm}_x(t)| \right) = \infty. \quad (42)$$

Proof For a contradiction, we assume that $|\text{Rm}_x(t)|$ is bounded by a constant. It follows from Corollary 25 that the metrics $g(t)$ converges smoothly to a smooth metric $g(T)$. Based on Theorem 23, it is possible to find a solution to the Ricci flow on $t \in [0, T)$, as the smooth metric $g(T)$ is uniformly equivalent to the initial metric $g(0)$.

Hence, we can extend the solution of the Ricci flow after the time point $t = T$, which contradicts the choice of T as the maximal time for the existence of the Ricci flow on $[0, T)$. In other words, $|\text{Rm}_x(t)|$ is unbounded. ■

As approaching the singular time T , the Riemann curvature $|\text{Rm}|_{g(t)}$ becomes no longer convergent and tends to explode.

Appendix D. Proof for Short Time Convergence in LNE Manifolds

Definition 27 *(Deruelle and Kröncke, 2021) A complete LNE n -manifold (\mathcal{M}^n, g_0) is said to be linearly stable if the L^2 spectrum of the Lichnerowicz operator $L_{g_0} := \Delta_{g_0} + 2\text{Rm}(g_0)^*$ is in $(-\infty, 0]$ where Δ_{g_0} is the Laplacian, when L_{g_0} acting on d_{ij} satisfies*

$$\begin{aligned} L_{g_0}(d) &= \Delta_{g_0}d + 2\text{Rm}(g_0) * d \\ &= \Delta_{g_0}d + 2\text{Rm}(g_0)_{iklj}d_{mn}g_0^{km}g_0^{ln}. \end{aligned} \quad (43)$$

Definition 28 *(Deruelle and Kröncke, 2021) A n -manifold (\mathcal{M}^n, g_0) is said to be integrable if a neighbourhood of g_0 has a smooth structure.*

We rewrite the Ricci-DeTurck flow (20) as an evolution of the difference $d(t) := \bar{g}(t) - \bar{g}_0$, such that

$$\begin{aligned} \frac{\partial}{\partial t}d(t) &= \frac{\partial}{\partial t}\bar{g}(t) = -2\text{Ric}(\bar{g}(t)) + 2\text{Ric}(\bar{g}_0) + \mathcal{L}_{\frac{\partial \varphi'(t)}{\partial t}}\bar{g}_0 - \mathcal{L}_{\frac{\partial \varphi(t)}{\partial t}}\bar{g}(t) \\ &= \Delta d(t) + \text{Rm} * d(t) + F_{\bar{g}^{-1}} * \nabla^{\bar{g}_0}d(t) * \nabla^{\bar{g}_0}d(t) + \nabla^{\bar{g}_0}(G_{\Gamma(\bar{g}_0)} * d(t) * \nabla^{\bar{g}_0}d(t)), \end{aligned} \quad (44)$$

where the tensors F and G depend on \bar{g}^{-1} and $\Gamma(\bar{g}_0)$. Note that \bar{g}_0 is the LNE metric which satisfies the above formula.

In the following, we denote $\|\cdot\|_{L^2}$ or $\|\cdot\|_{L^\infty}$ as the L^2 -norm or L^∞ -norm w.r.t. the LNE metric \bar{g}_0 , and mark generic constants as C or C_1 .

Lemma 29 *Let $(\mathcal{M}^n, \bar{g}_0)$ be a complete Ricci-flat n -manifold. If $\bar{g}(0)$ is a metric satisfying $\|\bar{g}(0) - \bar{g}_0\|_{L^\infty} < \epsilon$ where $\epsilon > 0$, then there exists a constant $C < \infty$ and a unique Ricci-DeTurck flow $\bar{g}(t)$ that satisfies*

$$\|\bar{g}(t) - \bar{g}_0\|_{L^\infty} < C\|\bar{g}(0) - \bar{g}_0\|_{L^\infty} < C \cdot \epsilon. \quad (45)$$

Proof The same statement is given in (Deruelle and Kröncke, 2021). The proofs can refer the details (Bamler, 2010, 2011). \blacksquare

Lemma 30 *Let $(\mathcal{M}^n, \bar{g}_0)$ be the LNE n -manifold. For a Ricci-DeTurck flow $\bar{g}(t)$ on a maximal time interval $t \in [0, T)$, if it satisfies $\|\bar{g}(0) - \bar{g}_0\|_{L^\infty} < \epsilon$ where $\epsilon > 0$, then there exists a constant $C < \infty$ for $t \in (0, T)$ such that*

$$\|\bar{g}(t) - \bar{g}_0\|_{L^2} \leq C. \quad (46)$$

Proof Based on Lemma 29, we can consider $\|\bar{g}(t) - \bar{g}_0\|_{L^2}$. Let κ be a function such that $\kappa = 1$ on $B(x, r)$, $\kappa = 0$ on $\mathcal{M}^n \setminus B(x, 2r)$ and $|\nabla\kappa| \leq 2/r$ where $x \in \mathcal{M}^n$ and a radius r .

Followed by Equation (44), we obtain

$$\begin{aligned} \frac{\partial}{\partial t} \int_{\mathcal{M}} |d(t)|^2 \kappa^2 d\mu &\leq 2 \int_{\mathcal{M}} \langle \Delta d(t), \kappa^2 d(t) \rangle d\mu + C \|\text{Rm}\|_{L^\infty} \int_{\mathcal{M}} |d(t)|^2 \kappa^2 d\mu \\ &\quad + C \|d(t)\|_{L^\infty} \int_{\mathcal{M}} |\nabla d(t)|^2 \kappa^2 d\mu + \int_{\mathcal{M}} \langle \nabla(G_\Gamma * d * \nabla d), d \rangle \kappa^2 d\mu \\ &\leq -2 \int_{\mathcal{M}} |\nabla d(t)|^2 \kappa^2 d\mu + C \int_{\mathcal{M}} |\nabla d(t)| |d(t)| |\nabla\kappa| \kappa d\mu \\ &\quad + C(\bar{g}_0) \int_{\mathcal{M}} |d(t)|^2 \kappa^2 d\mu + C \|d(t)\|_{L^\infty} \int_{\mathcal{M}} |\nabla d(t)|^2 \kappa^2 d\mu \\ &\leq (-2 + C \cdot \epsilon + C_1) \int_{\mathcal{M}} |\nabla d(t)|^2 \kappa^2 d\mu + C(\bar{g}_0) \int_{\mathcal{M}} |d(t)|^2 \kappa^2 d\mu \\ &\quad + \frac{1}{C_1} \int_{\mathcal{M}} |d(t)|^2 |\nabla\kappa|^2 d\mu \\ &\leq \left(C(\bar{g}_0) + \frac{2}{C_1 r^2} \right) \int_{B(x, 2r)} |d(t)|^2 d\mu. \end{aligned}$$

Note that we can always find a suitable C_1 to make the above formula true. By integration in time t , we can further obtain

$$\int_{\mathcal{M}} |d(t)|^2 \kappa^2 d\mu \leq \int_{\mathcal{M}} |d(0)|^2 \kappa^2 d\mu + \left(C(\bar{g}_0) + \frac{2}{C_1 r^2} \right) \int_0^t \int_{B(x, 2r)} |d(s)|^2 d\mu ds < \infty.$$

Consequently, we can find a finite ball that satisfies this estimate. \blacksquare

Appendix E. Proof for Long Time Stability in LNE Manifolds

Lemma 31 *Let $\bar{g}(t)$ be a Ricci–DeTurck flow on a maximal time interval $t \in (0, T)$ in an L^2 -neighbourhood of \bar{g}_0 . We have the following estimate:*

$$\left\| \frac{\partial}{\partial t} d_0(t) \right\|_{L^2} \leq C \left\| \nabla^{\bar{g}_0(t)} (d(t) - d_0(t)) \right\|_{L^2}^2. \quad (47)$$

Proof According to the Hardy inequality (Minerbe, 2009), we have the same proofs by referring the details (Deruelle and Kröncke, 2021). \blacksquare

Theorem 32 *Let $(\mathcal{M}^n, \bar{g}_0)$ be the LNE n -manifold which is linearly stable and integrable. Then, there exists a constant $\alpha_{\bar{g}_0}$ satisfying*

$$(\Delta d(t) + \text{Rm}(\bar{g}_0) * d(t), d(t))_{L^2} \leq -\alpha_{\bar{g}_0} \left\| \nabla^{\bar{g}_0} d(t) \right\|_{L^2}^2 \quad (48)$$

for all $\bar{g}(t) \in \tilde{\mathcal{F}}$ whose definition is given in Equation (22).

Proof The similar proofs can be found in (Devyver, 2014) with some minor modifications. Due to the linear stability requirement of LNE manifolds in Definition 27, $-L_{\bar{g}_0}$ is non-negative. Then there exists a positive constant $\alpha_{\bar{g}_0}$ satisfying

$$\alpha_{\bar{g}_0} (-\Delta d(t), d(t))_{L^2} \leq (-\Delta d(t) - \text{Rm}(\bar{g}_0) * d(t), d(t))_{L^2}.$$

By Taylor expansion, we repeatedly use elliptic regularity and Sobolev embedding (Pacini, 2010) to obtain the estimate. \blacksquare

Corollary 33 *Let $(\mathcal{M}^n, \bar{g}_0)$ be the LNE n -manifold which is integrable. For a Ricci–DeTurck flow $\bar{g}(t)$ on a maximal time interval $t \in [0, T]$, if it satisfies $\|\bar{g}(t) - \bar{g}_0\|_{L^\infty} < \epsilon$ where $\epsilon > 0$, then there exists a constant $C < \infty$ for $t \in [0, T]$ such that the evolution inequality satisfies*

$$\|d(t) - d_0(t)\|_{L^2}^2 \geq C \int_0^t \left\| \nabla^{\bar{g}_0(s)} (d(s) - d_0(s)) \right\|_{L^2}^2 dt. \quad (49)$$

Proof Based on Equation (44), we know

$$\begin{aligned} \frac{\partial}{\partial t} (d(t) - d_0) &= \Delta(d(t) - d_0) + \text{Rm} * (d(t) - d_0) \\ &\quad + F_{\bar{g}^{-1}} * \nabla^{\bar{g}_0} (d(t) - d_0) * \nabla^{\bar{g}_0} (d(t) - d_0) \\ &\quad + \nabla^{\bar{g}_0} (G_{\Gamma(\bar{g}_0)} * (d(t) - d_0) * \nabla^{\bar{g}_0} (d(t) - d_0)). \end{aligned}$$

Followed by Lemma 31 and Theorem 32, we further obtain

$$\begin{aligned}
 \frac{\partial}{\partial t} \|d(t) - d_0\|_{L^2}^2 &= 2 (\Delta(d(t) - d_0) + \text{Rm} * (d(t) - d_0), d(t) - d_0)_{L^2} \\
 &\quad + (F_{\bar{g}^{-1}} * \nabla^{\bar{g}_0}(d(t) - d_0) * \nabla^{\bar{g}_0}(d(t) - d_0), d(t) - d_0)_{L^2} \\
 &\quad + (\nabla^{\bar{g}_0}(G_{\Gamma(\bar{g}_0)} * (d(t) - d_0) * \nabla^{\bar{g}_0}(d(t) - d_0)), d(t) - d_0)_{L^2} \\
 &\quad + \left(d(t) - d_0, \frac{\partial}{\partial t} d_0(t) \right)_{L^2} + \int_{\mathcal{M}} (d(t) - d_0) * (d(t) - d_0) * \frac{\partial}{\partial t} d_0(t) d\mu \\
 &\leq -2\alpha_{\bar{g}_0} \|\nabla^{\bar{g}_0}(d(t) - d_0)\|_{L^2}^2 \\
 &\quad + C \|d(t) - d_0\|_{L^\infty} \|\nabla^{\bar{g}_0}(d(t) - d_0)\|_{L^2}^2 \\
 &\quad + \left\| \frac{\partial}{\partial t} d_0(t) \right\|_{L^2} \|d(t) - d_0\|_{L^2} \\
 &\leq (-2\alpha_{\bar{g}_0} + C \cdot \epsilon) \|\nabla^{\bar{g}_0}(d(t) - d_0)\|_{L^2}^2.
 \end{aligned}$$

Let ϵ be a small enough constant that $-2\alpha_{\bar{g}_0} + C \cdot \epsilon < 0$ holds, we can find

$$\frac{\partial}{\partial t} \|d(t) - d_0\|_{L^2}^2 \leq -C \|\nabla^{\bar{g}_0}(d(t) - d_0)\|_{L^2}^2$$

holds. ■

Definition 34 (Sheridan and Rubinstein, 2006) *Let $\bar{g}(t)$ be the metrics on the LNE manifold. For $\epsilon > 0$, $\mathcal{B}_{L^2}(\bar{g}_0, \epsilon)$ is the ϵ -ball with respect to the L^2 -norm induced by \bar{g}_0 and centred at \bar{g}_0 , where any metric $\bar{g}(t) \in \mathcal{B}_{L^2}(\bar{g}_0, \epsilon)$ is ϵ -close to \bar{g}_0 if*

$$(1 + \epsilon)^{-1} \bar{g}_0 \leq \bar{g}(t) \leq (1 + \epsilon) \bar{g}_0 \tag{50}$$

in the sense of matrices.

Appendix F. Proof for the Information Geometry

F.1 Proof for Theorem 9

The LNE divergence can be defined between two nearby points ξ and ξ' , where the first derivative of the LNE divergence w.r.t. ξ' is:

$$\begin{aligned}
 &\partial_{\xi'} D_{LNE}[\xi' : \xi] \\
 &= \sum_i \left[\partial_{\xi'_i} \frac{1}{\tau^2} \log \cosh(\tau \xi'_i) - \partial_{\xi'_i} \frac{1}{\tau^2} \log \cosh(\tau \xi_i) - \frac{1}{\tau} \partial_{\xi'_i} (\xi'_i - \xi_i) \tanh(\tau \xi_i) \right] \\
 &= \sum_i \partial_{\xi'_i} \frac{1}{\tau^2} \log \cosh(\tau \xi'_i) - \frac{1}{\tau} \tanh(\tau \xi).
 \end{aligned}$$

The second derivative of the LNE divergence w.r.t. ξ' is:

$$\partial_{\xi'}^2 D_{LNE}[\xi' : \xi] = \sum_i \partial_{\xi'_i}^2 \frac{1}{\tau^2} \log \cosh(\tau \xi'_i).$$

We deduce the Taylor expansion of the LNE divergence at $\boldsymbol{\xi}' = \boldsymbol{\xi}$:

$$\begin{aligned}
 D_{LNE}[\boldsymbol{\xi}' : \boldsymbol{\xi}] &\approx D_{LNE}[\boldsymbol{\xi} : \boldsymbol{\xi}] + \left(\sum_i \partial_{\xi'_i} \frac{1}{\tau^2} \log \cosh(\tau \xi'_i) - \frac{1}{\tau} \tanh(\tau \boldsymbol{\xi}) \right) \Big|_{\boldsymbol{\xi}'=\boldsymbol{\xi}}^\top d\boldsymbol{\xi} \\
 &+ \frac{1}{2} d\boldsymbol{\xi}^\top \left(\sum_i \partial_{\xi'_i}^2 \frac{1}{\tau^2} \log \cosh(\tau \xi'_i) \right) \Big|_{\boldsymbol{\xi}'=\boldsymbol{\xi}} d\boldsymbol{\xi} \\
 &= 0 + 0 + \frac{1}{2\tau^2} d\boldsymbol{\xi}^\top \partial \left[\frac{\partial \cosh(\tau \boldsymbol{\xi})}{\cosh(\tau \boldsymbol{\xi})} \right] d\boldsymbol{\xi} \\
 &= \frac{1}{2\tau^2} d\boldsymbol{\xi}^\top \frac{\partial^2 \cosh(\tau \boldsymbol{\xi}) \cosh(\tau \boldsymbol{\xi}) - \partial \cosh(\tau \boldsymbol{\xi}) \partial \cosh(\tau \boldsymbol{\xi})}{\cosh^2(\tau \boldsymbol{\xi})} d\boldsymbol{\xi} \\
 &= \frac{1}{2\tau^2} d\boldsymbol{\xi}^\top \left(\frac{\partial^2 \cosh(\tau \boldsymbol{\xi})}{\cosh(\tau \boldsymbol{\xi})} - \tau^2 \left[\frac{\sinh(\tau \boldsymbol{\xi})}{\cosh(\tau \boldsymbol{\xi})} \right] \left[\frac{\sinh(\tau \boldsymbol{\xi})}{\cosh(\tau \boldsymbol{\xi})} \right]^\top \right) d\boldsymbol{\xi} \\
 &= \frac{1}{2} \sum_{i,j} \delta_{ij} - \left[\tanh(\tau \boldsymbol{\xi}) \tanh(\tau \boldsymbol{\xi})^\top \right]_{ij} d\xi_i d\xi_j.
 \end{aligned}$$

F.2 Proof for Lemma 10

We would like to know in which direction minimizes the loss function with the constraints of the LNE divergence, so that we do the minimization:

$$d\boldsymbol{\xi}^* = \underset{d\boldsymbol{\xi} \text{ s.t. } D_{LNE}[\boldsymbol{\xi}:\boldsymbol{\xi}+d\boldsymbol{\xi}]=c}{\arg \min} L(\boldsymbol{\xi} + d\boldsymbol{\xi})$$

where c is the constant. The loss function descends along the manifold with constant speed, regardless the curvature.

Furthermore, we can write the minimization in Lagrangian form. Combined with Theorem 9, the LNE divergence can be approximated by its second order Taylor expansion. Approximating $L(\boldsymbol{\xi} + d\boldsymbol{\xi})$ with its first order Taylor expansion, we get:

$$\begin{aligned}
 d\boldsymbol{\xi}^* &= \arg \min_{d\boldsymbol{\xi}} L(\boldsymbol{\xi} + d\boldsymbol{\xi}) + \lambda (D_{LNE}[\boldsymbol{\xi} : \boldsymbol{\xi} + d\boldsymbol{\xi}] - c) \\
 &\approx \arg \min_{d\boldsymbol{\xi}} L(\boldsymbol{\xi}) + \partial_{\boldsymbol{\xi}} L(\boldsymbol{\xi})^\top d\boldsymbol{\xi} + \frac{\lambda}{2} d\boldsymbol{\xi}^\top g(\boldsymbol{\xi}) d\boldsymbol{\xi} - c\lambda.
 \end{aligned}$$

To solve this minimization, we set its derivative w.r.t. $d\boldsymbol{\xi}$ to zero:

$$\begin{aligned}
 0 &= \frac{\partial}{\partial d\boldsymbol{\xi}} L(\boldsymbol{\xi}) + \partial_{\boldsymbol{\xi}} L(\boldsymbol{\xi})^\top d\boldsymbol{\xi} + \frac{\lambda}{2} d\boldsymbol{\xi}^\top \left[\delta - \tanh(\tau \boldsymbol{\xi}) \tanh(\tau \boldsymbol{\xi})^\top \right] d\boldsymbol{\xi} - c\lambda \\
 &= \partial_{\boldsymbol{\xi}} L(\boldsymbol{\xi}) + \lambda \left[\delta - \tanh(\tau \boldsymbol{\xi}) \tanh(\tau \boldsymbol{\xi})^\top \right] d\boldsymbol{\xi} \\
 d\boldsymbol{\xi} &= -\frac{1}{\lambda} \left[\delta - \tanh(\tau \boldsymbol{\xi}) \tanh(\tau \boldsymbol{\xi})^\top \right]^{-1} \partial_{\boldsymbol{\xi}} L(\boldsymbol{\xi})
 \end{aligned}$$

where a constant factor $1/\lambda$ can be absorbed into learning rate. Therefore, we get the optimal descent direction, i.e., the opposite direction of gradient, which takes into account the local curvature defined by $\left[\delta - \tanh(\tau \boldsymbol{\xi}) \tanh(\tau \boldsymbol{\xi})^\top \right]^{-1}$.

References

- T. Ajanthan, K. Gupta, P. Torr, R. Hartley, and P. Dokania. Mirror descent view for neural network quantization. In *International Conference on Artificial Intelligence and Statistics*, pages 2809–2817. PMLR, 2021.
- S.-I. Amari. Natural gradient works efficiently in learning. *Neural computation*, 10(2): 251–276, 1998.
- S.-i. Amari. *Information geometry and its applications*, volume 194. Springer, 2016.
- S.-i. Amari and H. Nagaoka. Methods of information geometry, volume 191 of translations of mathematical monographs, s. kobayashi and m. takesaki, editors. *American Mathematical Society, Providence, RI, USA*, pages 2–19, 2000.
- A. Appleton. Scalar curvature rigidity and ricci deturck flow on perturbations of euclidean space. *Calculus of Variations and Partial Differential Equations*, 57(5):1–23, 2018.
- J. L. Ba, J. R. Kiros, and G. E. Hinton. Layer normalization. *arXiv preprint arXiv:1607.06450*, 2016.
- Y. Bai, Y.-X. Wang, and E. Liberty. Proxquant: Quantized neural networks via proximal operators. *arXiv preprint arXiv:1810.00861*, 2018.
- R. H. Bamler. Stability of hyperbolic manifolds with cusps under ricci flow. *arXiv preprint arXiv:1004.2058*, 2010.
- R. H. Bamler. *Stability of Einstein metrics of negative curvature*. Princeton University, 2011.
- M. Basseville. Divergence measures for statistical data processing—an annotated bibliography. *Signal Processing*, 93(4):621–633, 2013.
- A. Beck and M. Teboulle. Mirror descent and nonlinear projected subgradient methods for convex optimization. *Operations Research Letters*, 31(3):167–175, 2003.
- Y. Bengio, N. Léonard, and A. Courville. Estimating or propagating gradients through stochastic neurons for conditional computation. *arXiv preprint arXiv:1308.3432*, 2013.
- A. L. Besse. *Einstein manifolds*. Springer Science & Business Media, 2007.
- R. Bhatia. *Matrix analysis*, volume 169. Springer Science & Business Media, 2013.
- L. M. Bregman. The relaxation method of finding the common point of convex sets and its application to the solution of problems in convex programming. *USSR computational mathematics and mathematical physics*, 7(3):200–217, 1967.
- S. Bubeck et al. Convex optimization: Algorithms and complexity. *Foundations and Trends® in Machine Learning*, 8(3-4):231–357, 2015.

- Z. Cai, X. He, J. Sun, and N. Vasconcelos. Deep learning with low precision by half-wave gaussian quantization. In *Proceedings of the IEEE conference on computer vision and pattern recognition*, pages 5918–5926, 2017.
- J. Chen, L. Liu, Y. Liu, and X. Zeng. A learning framework for n-bit quantized neural networks toward fpgas. *IEEE Transactions on Neural Networks and Learning Systems*, pages 1–15, 2020. doi: 10.1109/TNNLS.2020.2980041.
- S. Chen, W. Wang, and S. J. Pan. Metaquant: Learning to quantize by learning to penetrate non-differentiable quantization. In *Advances in Neural Information Processing Systems*, volume 32, pages 3916–3926. Curran Associates, Inc., 2019.
- M. Courbariaux, I. Hubara, D. Soudry, R. El-Yaniv, and Y. Bengio. Binarized neural networks: Training deep neural networks with weights and activations constrained to+ 1 or-1. *arXiv preprint arXiv:1602.02830*, 2016.
- G. Cybenko. Approximation by superpositions of a sigmoidal function. *Mathematics of control, signals and systems*, 2(4):303–314, 1989.
- A. Deruelle and K. Kröncke. Stability of ale ricci-flat manifolds under ricci flow. *The Journal of Geometric Analysis*, 31(3):2829–2870, 2021.
- D. M. DeTurck. Deforming metrics in the direction of their ricci tensors. *Journal of Differential Geometry*, 18(1):157–162, 1983.
- B. Devyver. A gaussian estimate for the heat kernel on differential forms and application to the riesz transform. *Mathematische Annalen*, 358(1):25–68, 2014.
- T. Dozat. Incorporating nesterov momentum into adam. 2016.
- M. Elhoushi, Z. Chen, F. Shafiq, Y. H. Tian, and J. Y. Li. Deepshift: Towards multiplication-less neural networks. *arXiv preprint arXiv:1905.13298*, 2019.
- C. Guenther, J. Isenberg, and D. Knopf. Stability of the ricci flow at ricci-flat metrics. *Communications in Analysis and Geometry*, 10(4):741–777, 2002.
- P. Gysel, J. Pimentel, M. Motamedi, and S. Ghiasi. Ristretto: A framework for empirical study of resource-efficient inference in convolutional neural networks. *IEEE transactions on neural networks and learning systems*, 29(11):5784–5789, 2018.
- R. S. Hamilton et al. Three-manifolds with positive ricci curvature. *J. Differential geom*, 17(2):255–306, 1982.
- K. He, X. Zhang, S. Ren, and J. Sun. Deep residual learning for image recognition. In *Proceedings of the IEEE conference on computer vision and pattern recognition*, pages 770–778, 2016.
- S. Helgason. *Differential geometry and symmetric spaces*, volume 341. American Mathematical Soc., 2001.
- G. Hinton. Neural networks for machine learning. coursera,[video lectures], 2012.

- K. Hornik. Approximation capabilities of multilayer feedforward networks. *Neural networks*, 4(2):251–257, 1991.
- L. Hou, Q. Yao, and J. T. Kwok. Loss-aware binarization of deep networks. *arXiv preprint arXiv:1611.01600*, 2016.
- A. G. Howard, M. Zhu, B. Chen, D. Kalenichenko, W. Wang, T. Weyand, M. Andreetto, and H. Adam. Mobilenets: Efficient convolutional neural networks for mobile vision applications. *arXiv preprint arXiv:1704.04861*, 2017.
- S. Ioffe and C. Szegedy. Batch normalization: Accelerating deep network training by reducing internal covariate shift. *arXiv preprint arXiv:1502.03167*, 2015.
- V. Jejjala, D. K. M. Pena, and C. Mishra. Neural network approximations for calabi-yau metrics. *arXiv preprint arXiv:2012.15821*, 2020.
- T. Kato. *Perturbation theory for linear operators*, volume 132. Springer Science & Business Media, 2013.
- P. Kaul and B. Lall. Riemannian curvature of deep neural networks. *IEEE transactions on neural networks and learning systems*, 31(4):1410–1416, 2019.
- H. Koch and T. Lamm. Geometric flows with rough initial data. *Asian Journal of Mathematics*, 16(2):209–235, 2012.
- N. Koiso. Einstein metrics and complex structures. *Inventiones mathematicae*, 73(1):71–106, 1983.
- A. Krizhevsky, G. Hinton, et al. Learning multiple layers of features from tiny images. 2009.
- A. Krizhevsky, I. Sutskever, and G. E. Hinton. Imagenet classification with deep convolutional neural networks. In *Advances in neural information processing systems*, pages 1097–1105, 2012.
- O. A. Ladyzhenskaia, V. A. Solonnikov, and N. N. Ural'tseva. *Linear and quasi-linear equations of parabolic type*, volume 23. American Mathematical Soc., 1988.
- C. Leng, Z. Dou, H. Li, S. Zhu, and R. Jin. Extremely low bit neural network: Squeeze the last bit out with admm. In *Proceedings of the AAAI Conference on Artificial Intelligence*, volume 32, 2018.
- F. Li, B. Zhang, and B. Liu. Ternary weight networks. *arXiv preprint arXiv:1605.04711*, 2016.
- Z. Liu, B. Wu, W. Luo, X. Yang, W. Liu, and K.-T. Cheng. Bi-real net: Enhancing the performance of 1-bit cnns with improved representational capability and advanced training algorithm. In *Proceedings of the European conference on computer vision (ECCV)*, pages 722–737, 2018.

- C. Louizos, M. Reisser, T. Blankevoort, E. Gavves, and M. Welling. Relaxed quantization for discretized neural networks. In *International Conference on Learning Representations*, 2019. URL <https://openreview.net/forum?id=HkxjYoCqKX>.
- J. Martens and R. Grosse. Optimizing neural networks with kronecker-factored approximate curvature. In *International conference on machine learning*, pages 2408–2417, 2015.
- V. Minerbe. Weighted sobolev inequalities and ricci flat manifolds. *Geometric and Functional Analysis*, 18(5):1696–1749, 2009.
- T. Pacini. Desingularizing isolated conical singularities: uniform estimates via weighted sobolev spaces. *arXiv preprint arXiv:1005.3511*, 2010.
- A. Paszke, S. Gross, F. Massa, A. Lerer, J. Bradbury, G. Chanan, T. Killeen, Z. Lin, N. Gimelshein, L. Antiga, et al. Pytorch: An imperative style, high-performance deep learning library. *arXiv preprint arXiv:1912.01703*, 2019.
- H. Qin, R. Gong, X. Liu, M. Shen, Z. Wei, F. Yu, and J. Song. Forward and backward information retention for accurate binary neural networks. In *Proceedings of the IEEE/CVF conference on computer vision and pattern recognition*, pages 2250–2259, 2020.
- G. Raskutti and S. Mukherjee. The information geometry of mirror descent. *IEEE Transactions on Information Theory*, 61(3):1451–1457, 2015.
- M. Rastegari, V. Ordonez, J. Redmon, and A. Farhadi. Xnor-net: Imagenet classification using binary convolutional neural networks. In *European conference on computer vision*, pages 525–542. Springer, 2016.
- O. Russakovsky, J. Deng, H. Su, J. Krause, S. Satheesh, S. Ma, Z. Huang, A. Karpathy, A. Khosla, M. Bernstein, et al. Imagenet large scale visual recognition challenge. *International journal of computer vision*, 115(3):211–252, 2015.
- H. Sak, A. W. Senior, and F. Beaufays. Long short-term memory recurrent neural network architectures for large scale acoustic modeling. 2014.
- O. C. Schnürer, F. Schulze, and M. Simon. Stability of euclidean space under ricci flow. *arXiv preprint arXiv:0706.0421*, 2007.
- N. Sesum. Linear and dynamical stability of ricci-flat metrics. *Duke Mathematical Journal*, 133(1):1–26, 2006.
- N. Sheridan and H. Rubinstein. Hamilton’s ricci flow. *Honour thesis*, 2006.
- C. Shorten and T. M. Khoshgoftaar. A survey on image data augmentation for deep learning. *Journal of big data*, 6(1):1–48, 2019.
- R. M. Wald. *General relativity*. University of Chicago press, 2010.
- J. Yang, X. Shen, J. Xing, X. Tian, H. Li, B. Deng, J. Huang, and X.-s. Hua. Quantization networks. In *Proceedings of the IEEE/CVF Conference on Computer Vision and Pattern Recognition (CVPR)*, June 2019.

- A. Zhou, A. Yao, Y. Guo, L. Xu, and Y. Chen. Incremental network quantization: Towards lossless cnns with low-precision weights. *arXiv preprint arXiv:1702.03044*, 2017.
- A. Zhou, A. Yao, K. Wang, and Y. Chen. Explicit loss-error-aware quantization for low-bit deep neural networks. In *Proceedings of the IEEE conference on computer vision and pattern recognition*, pages 9426–9435, 2018.
- S. Zhou, Y. Wu, Z. Ni, X. Zhou, H. Wen, and Y. Zou. Dorefa-net: Training low bitwidth convolutional neural networks with low bitwidth gradients. *arXiv preprint arXiv:1606.06160*, 2016.
- C. Zhu, S. Han, H. Mao, and W. J. Dally. Trained ternary quantization. *arXiv preprint arXiv:1612.01064*, 2016.
- F. Zhu, R. Gong, F. Yu, X. Liu, Y. Wang, Z. Li, X. Yang, and J. Yan. Towards unified int8 training for convolutional neural network. In *Proceedings of the IEEE/CVF Conference on Computer Vision and Pattern Recognition*, pages 1969–1979, 2020.